RESEARCH ARTICLE SUMMARY

PLANT SCIENCE

Evolution of interorganismal strigolactone biosynthesis in seed plants

Anqi Zhou†, Annalise Kane†, Sheng Wu, Kaibiao Wang, Michell Santiago, Yui Ishiguro, Kaori Yoneyama, Malathy Palayam, Nitzan Shabek, Xiaonan Xie*, David C. Nelson*, Yanran Li*

BACKGROUND: Plant development and adaptive responses to the environment are regulated by small, mobile molecules known as hormones. Strigolactones are a class of plant hormones that control many traits, including shoot and root architecture, senescence, drought tolerance, and cambial growth. However, strigolactones may have originally served as signals for interorganismal communication, rather than as hormones. Plants exude strigolactones from roots, particularly during low nitrogen or phosphorus availability, which recruits symbiotic interactions with microbes that can alleviate nutrient deficiencies. A downside of this strategy is that many parasitic plants that attach to roots, including several major agricultural weeds, evolved to use strigolactones as germination cues and/or for chemotropic growth toward a host.

Perhaps because of evolutionary pressures from these plant-biotic interactions, plants collectively produce a diverse array of strigolactones. The strigolactone family is divided by structural differences into canonical strigolactones, which primarily have external signaling roles, and noncanonical strigolactones, which are believed to primarily serve as hormones. Both classes share a common precursor, carlactonoic acid (CLA), that is formed from all-*trans*-β-carotene (ATβC). The initial conversion of CLA to canonical strigolactones is carried out by cytochrome P450 enzymes. In most flowering plants, this reaction is catalyzed by proteins in the CYP722C clade. Several other enzymes have been found to diversify strigolactone structures, but the biosynthesis and specific functions of many strigolactones remain unresolved.

RATIONALE: We hypothesized that CYP722C homologs might also produce strigolactones. CYP722A and monocot-specific CYP722B proteins form an uncharacterized sister clade to CYP722C that is widely distributed in seed plants. Functional investigations of CYP722A/B proteins and other candidate strigolactone biosynthesis enzymes are complicated by the limited availability or stability of likely substrates, such as CLA, the unknown nature of their metabolic products, and the low abundance of strigolactones in plants. New approaches are required to bypass these limitations.

The development of microbial cell factories through synthetic biology and metabolic engineering strategies has greatly facilitated access to chemical substrates and products, simplifying the characterization of enzymes and the structural elucidation of previously unidentified metabolites. Furthermore, authentic standards provided by microbial cell factories and advances in targeted metabolomics technologies now enable detection of low-abundance compounds in plant samples with greater reliability and clarity. We took advantage of these tools to investigate CYP722A function.

RESULTS: We optimized a microbial consortium that expresses the core plant strigolactone biosynthesis pathway in *Escherichia coli* and *Saccharomyces cerevisiae* hosts to yield 125-fold greater titers of a canonical strigolactone. Coexpression of *CYP722A* and *CYP722B* genes from 16 plant species in the consortium produced a previously unidentified compound from CLA that was determined to be a noncanonical strigolactone, 16-hydroxy-carlactonoic acid (16-OH-CLA). We detected 16-OH-CLA only in the shoot tissues of plants, in contrast to other known strigolactones.

16-OH-CLA shows strigolactone properties in vivo. It suppresses axillary shoot branching in strigolactone-deficient *Arabidopsis thaliana* plants and signals through the strigolactone receptor DWARF14. Unexpectedly, 16-OH-CLA deficiency has no effect on shoot branching. We discovered that 16-OH-CLA activity in seedlings requires genes involved in noncanonical strigolactone biosynthesis, *CARLACTONOIC ACID METHYLTRANSFERASE* (*CLAMT*) and *LATERAL BRANCHING OXIDOREDUCTASE* (*LBO*). In the microbial consortium, the sequential action of CLAMT and LBO consumes 16-OH-CLA, producing methyl 16-hydroxycarlactonoate and an unknown metabolite. Because CLAMT also uses CLA as a substrate, we hypothesize that CLA shunts into CLAMT- and LBO-mediated metabolism to compensate for the loss of *CYP722A* in *Arabidopsis*.

We used structural models to identify candidate residues that differentiate the activities of CYP722A and CYP722C on CLA. A single amino acid change in the active site of CYP722A proteins gains production of 18-OH-CLA, an intermediate in canonical strigolactone formation by CYP722C.

CONCLUSION: The evolution of CYP722C proteins from CYP7722A was a key transition in strigolactone biosynthesis by seed-bearing plants. A change in the site of CLA oxidation led to emergence of a class of strigolactones that mediate plant-biotic interactions. ■

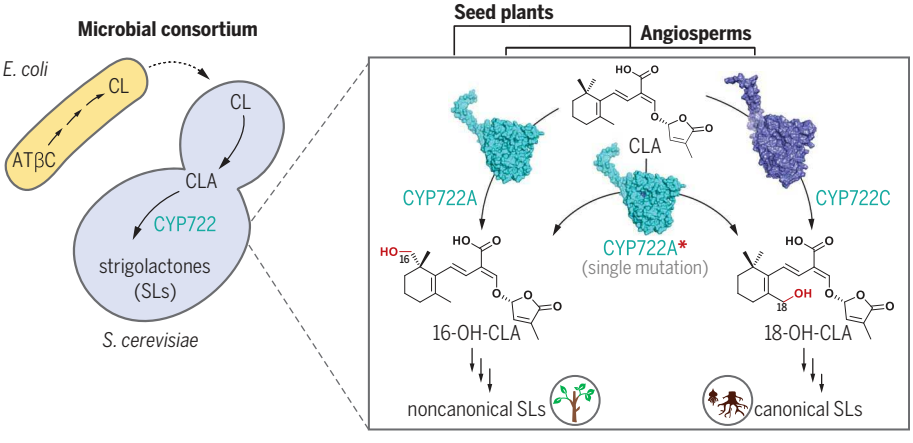

Synthetic biology–enabled characterization of strigolactone biosynthesis genes. An engineered microbial consortium reconstitutes strigolactone biosynthesis. CYP722A proteins are homologous to CYP722C in angiosperms. CYP722A oxidizes CLA at C16, whereas CYP722C oxidizes CLA at C18. These intermediates are converted to noncanonical strigolactones or canonical strigolactones that signal to other organisms in soil, respectively. A single mutation enables both types of oxidations. CL, carlactone; SL, strigolactone.

The list of author affiliations is available in the full article online.
*Corresponding author. Email: yanl152@ucsd.edu (Y.L.); david.nelson@ucr.edu (D.C.N.); xie@cc.utsunomiya-u.ac.jp (X.X.)
†These authors contributed equally to this work.
Cite this article as A. Zhou *et al.*, *Science* **387**, eadp0779 (2025). DOI: 10.1126/science.adp0779

READ THE FULL ARTICLE AT
https://doi.org/10.1126/science.adp0779

RESEARCH ARTICLE

PLANT SCIENCE

Evolution of interorganismal strigolactone biosynthesis in seed plants

Anqi Zhou[1]†, Annalise Kane[2]†, Sheng Wu[3], Kaibiao Wang[1], Michell Santiago[2], Yui Ishiguro[4], Kaori Yoneyama[5], Malathy Palayam[6], Nitzan Shabek[6], Xiaonan Xie[4]*, David C. Nelson[2]*, Yanran Li[1]*

Strigolactones (SLs) are methylbutenolide molecules derived from β-carotene through an intermediate carlactonoic acid (CLA). Canonical SLs act as signals to microbes and plants, whereas noncanonical SLs are primarily plant hormones. The cytochrome P450 CYP722C catalyzes a critical step, converting CLA to canonical SLs in most angiosperms. Using synthetic biology, we investigated the function of *CYP722A*, an evolutionary predecessor of *CYP722C*. CYP722A converts CLA into 16-hydroxy-CLA (16-OH-CLA), a noncanonical SL detected exclusively in the shoots of various flowering plants. 16-OH-CLA application restores control of shoot branching to SL-deficient mutants in *Arabidopsis thaliana* and is perceived by the SL signaling pathway. We hypothesize that biosynthesis of 16-OH-CLA by CYP722A was a metabolic stepping stone in the evolution of canonical SLs that mediate rhizospheric signaling in many flowering plants.

Strigolactones (SLs) are a diverse family of apocarotenoids that play important roles in the regulation of plant development and plant-biotic interactions (*1*). As hormones, SLs control axillary branch growth (tillering), stem elongation, leaf morphology, and drought tolerance (*2*, *3*). SLs also regulate plant susceptibility to pathogenic microbes and root-knot nematodes (*4*). As interorganismal signals, SLs are exuded into the soil, particularly when nitrogen or phosphorus availability is low, where they promote beneficial symbiotic associations with arbuscular mycorrhizal fungi (AMF) and rhizobacteria (*4*). Root parasitic plants in the Orobanchaceae (for example, *Striga* spp.) use SLs to trigger germination and growth toward a host (*5*, *6*).

SLs feature a methylbutenolide "D-ring" conjugated to a variable scaffold through an enol-ether linkage. SLs are divided into canonical or noncanonical classes on the basis of the scaffold having a tricyclic "ABC"-ring structure or not, respectively (Fig. 1A). Canonical SLs are primarily used as interorganismal signals, whereas noncanonical SLs have a predominant role in hormone signaling within the plant (*7*–*10*). During SL perception, the D-ring is cleaved and covalently attached to catalytic triad residues in the α/β-hydrolase enzyme receptor DWARF14 (D14) (*11*, *12*). Activation of D14 promotes its association with the F-box protein MORE AXILLARY GROWTH2 (MAX2)/DWARF3 (D3) and DWARF53 (D53)–type proteins in the SUPPRESSOR OF MAX2 1-LIKE (SMXL) family. Subsequent polyubiquitination and proteasomal degradation of these SMXL proteins activate downstream growth responses (*3*). More than 30 SLs have been identified from plants, almost all of which were isolated from roots or root exudates (*13*).

SL biosynthesis begins with the conversion of all-*trans*-β-carotene into carlactone (CL) through the sequential actions of a β-carotene isomerase [DWARF27 (D27)] and two carotenoid cleavage dioxygenases, CCD7 and CCD8 (Fig. 1A) (*14*). CL is then converted to carlactonoic acid (CLA) by a cytochrome P450, CYP711A1 [also known as MORE AXILLARY GROWTH1 (MAX1)]. In some plants, such as rice (*Oryza sativa*) and peach (*Prunus persica*), paralogs of MAX1 catalyze the conversion of CL to canonical SLs through CLA (*15*, *16*). More often, CLA is processed further by other enzymes (Fig. 1A and fig. S1). Noncanonical SLs such as methyl-CLA (MeCLA) and hydroxymethyl carlactonoate (1′-OH-MeCLA) are made by CARLACTONOIC ACID METHYLTRANSFERASE (CLAMT) and LATERAL BRANCHING OXIDOREDUCTASE (LBO), respectively (*17*–*19*). Canonical SLs such as orobanchol (ORO) or 5-deoxystrigol (5DS) are formed from CLA through CYP722C proteins in many flowering plants (*7*, *20*–*22*). One type of CYP722C forms 5DS directly from an 18-hydroxy-CLA (18-OH-CLA) intermediate. Another type performs a second oxidation step that makes 18-oxo-CLA, which can spontaneously cyclize under acidic conditions but is stereospecifically converted to ORO by STEREOSELECTIVE RING FACTOR (SRF) (*23*).

Although CYP711A/MAX1 enzymes in rice were the first to be implicated in the direct synthesis of canonical SLs (*15*), subsequent surveys have shown that such activity is uncommon among MAX1 proteins and, so far, only found in species with multiple *MAX1* copies (*16*, *24*, *25*). Notably, *MAX1* is maintained as a single gene copy in most plants (*26*). By contrast, CYP722C proteins from many species have consistently been observed to produce canonical SLs through catalyzing C18-oxidation of CLA (*7*, *20*–*22*). Therefore, in most flowering plants and especially dicots, CYP722C proteins are likely to be critical for making the SLs used in communication with microbes and other plants. We set out to investigate the evolution of this mechanism of canonical SL biosynthesis.

CYP722A/B produces an unknown metabolite from CLA

Phylogenetic analysis revealed two uncharacterized sister clades to *CYP722C* in seed plants (embryophytes), *CYP722A* and *CYP722B* (fig. S2A). To investigate the metabolic functions of CYP722A and CYP722B, we took advantage of a microbial consortium system for heterologous biosynthesis of SLs that we recently developed (Fig. 1B). In this system, a set of engineered *Escherichia coli* and *Saccharomyces cerevisiae* strains expressing plant SL biosynthetic enzymes are cocultured to produce a range of SLs and related molecules, including CL, CLA, ORO, 5DS, 18-OH-CLA, 4-deoxyorobanchol, and strigol (*16*, *21*, *24*). The system facilitates efficient identification and functional characterization of SL biosynthetic enzymes (*16*, *21*, *24*). We synthesized yeast-codon–optimized *CYP722A/B* coding sequences from eudicot plants *Arabidopsis thaliana* (*AtCYP722A*) and peach (*PpCYP722A*); basal eudicot *Aquilegia coerulea* (*AcCYP722A*); and a monocot, rice (*OsCYP722B*). Each gene was coexpressed with *CYTOCHROME P450 REDUCTASE 1* (*ATR1*) and MAX1 (*AtMAX1*) from *A. thaliana* in *S. cerevisiae* CEN.PK2-1D, forming yeast SL-producing strains YSL2 to YSL5 (table S2). These strains were cocultured with an *E. coli* CL–producing strain (ECL1) (table S2) that supplies the substrate (*21*). A new peak with a retention time (RT) of 12.32 min was detected by means of liquid chromatography–mass spectrometry (LC-MS) in all microbial consortia expressing *CYP722A* or *CYP722B* (ECL1/YSL2-5) (Fig. 1C and table S2). The peak had a negative mass/charge ratio (*m*/*z*) at 347.1, which is consistent with the mass of an oxidized CLA molecule (+16 Da). Supporting this hypothesis, the reduced RT of the peak compared with that of CLA (16.81 min) implied that the CYP722A/B metabolite was more hydrophilic than CLA and likely a hydroxylated CLA molecule that

[1]Aiiso Yufeng Li Family Department of Chemical and Nano Engineering, University of California, San Diego, CA, USA. [2]Department of Botany and Plant Sciences, University of California, Riverside, CA, USA. [3]The Research Center of Chiral Drugs, Innovation Research Institute of Traditional Chinese Medicine, Shanghai University of Traditional Chinese Medicine, Shanghai, China. [4]Center for Bioscience Research and Education, Utsunomiya University, Tochigi, Japan. [5]Department Research and Development Bureau, Saitama University, Saitama-shi, Japan. [6]Department of Plant Biology, College of Biological Sciences, University of California, Davis, CA, USA.
*Corresponding author. Email: yanl152@ucsd.edu (Y.L.); david.nelson@ucr.edu (D.C.N.); xie@cc.utsunomiya-u.ac.jp (X.X.)
†These authors contributed equally to this work.

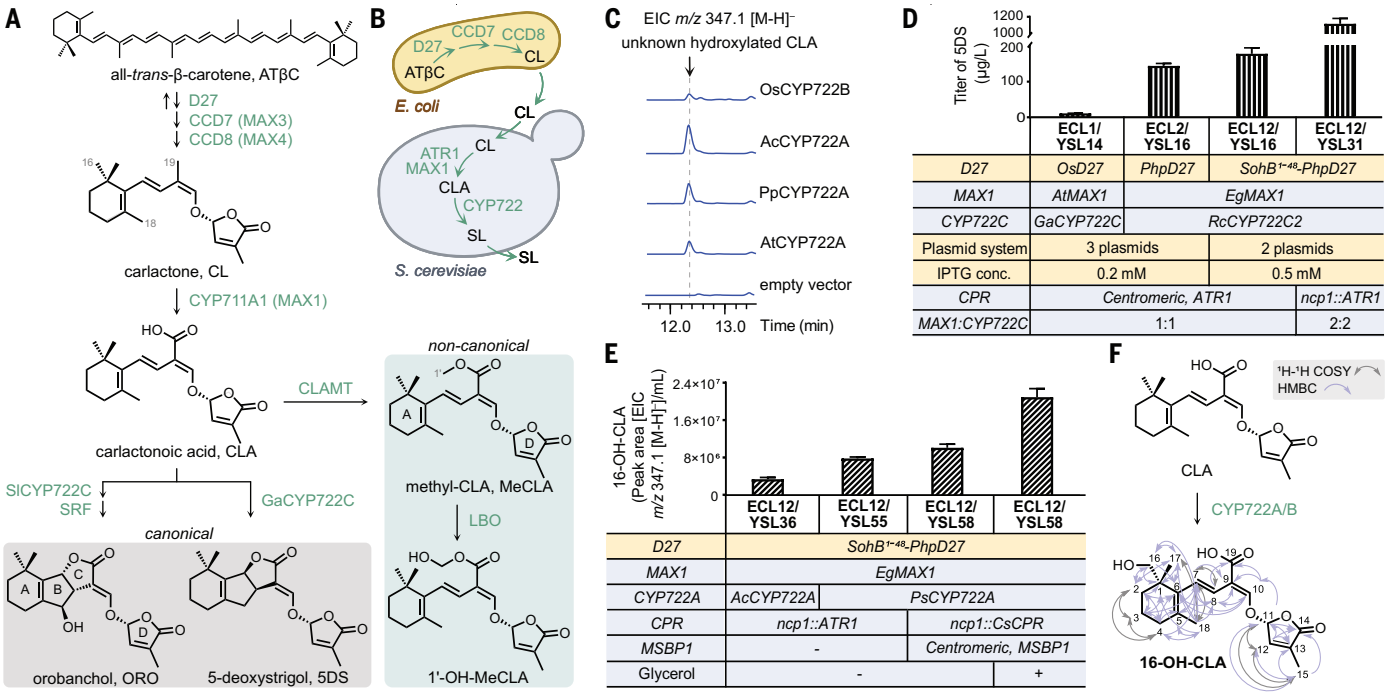

Fig. 1. Functional characterization of CYP722A/B by using SL-producing microbial consortia. (**A**) Biosynthesis of SLs in seed plants. (**B**) Illustration of SL-producing *E. coli*–*S. cerevisiae* consortium. (**C**) Functional characterization of CYP722A/Bs by using the microbial consortium. LC-MS selected ion monitoring (SIM) extracted ion chromatogram (EIC) at hydroxylated CLA's characteristic $[M\text{-}H]^-$ *m/z* 347.1 (MW = 332.4 + 16 Da = 348.4 Da) of CL-accumulating *E. coli* ECL1 cocultured with ATR1- and AtMAX1-expressing *S. cerevisiae* harboring a plasmid expressing different CYP722A/B or empty vector as a negative control. (**D**) Optimization of the production efficiency of the SL-producing microbial consortia by using 5DS as the calibration method. Detailed engineering strategies and experimental details on 5DS production optimization can be found in section "Detailed engineering strategies to enhance 5DS production" and figs. S4 to S6. (**E**) Further engineering of the consortia for enhanced production of CYP722A/B metabolite. Detailed experimental data on 16-OH-CLA production optimization can be found in fig. S7. (**F**) Structural elucidation of 16-OH-CLA by using NMR analysis. Gray and purple arrows indicate observed ^{1}H-^{1}H-COSY and ^{1}H-^{13}C-HMBC coupling, respectively.

was oxidized on a different carbon than the CYP722C product, 18-OH-CLA (RT 12.54 min). To determine whether the CYP722A/B metabolite was produced from CLA or CL, microbial consortia were tested without coexpression of *AtMAX1* (ECL1/YSL6-7) (tables S2). The CYP722A/B metabolite was not detected when only CL was present, indicating that CLA is the true substrate of CYP722A/B (fig. S3).

Enhancing microbial consortium performance through metabolic engineering

Because the yield of the previously developed microbial consortium would be insufficient for the isolation and structural elucidation of the CYP722A/B metabolite (*21*), we set out to optimize its efficiency. We used the titer of 5DS as a benchmark for optimization because it can be quantified by using an authentic standard. Our optimization strategies included testing *D27*, *MAX1*, and *CYP722C* variants from different species; making *N*-terminal modifications to the gatekeeper enzyme D27; packaging *D27*, *CCD7*, and *CCD8* on a single plasmid; altering fermentation conditions; inactivating yeast endogenous CPR; and increasing the copy numbers of *MAX1* and *CYP722C* (figs. S4 to S6). These efforts led to a 125.6-fold increase in 5DS titer, from 8.85 μg/liter in ECL1/YSL14 to 1.12 mg/liter in ECL12/YSL31 induced with 0.5 mM isopropyl β-D-1-thiogalactopyranoside (IPTG) (Fig. 1D and table S2).

CYP722A/B synthesizes 16-hydroxy-carlactonoic acid

Building on the optimized conditions for 5DS synthesis, we produced the CYP722A/B metabolite by replacing *RcCYP722C2* with *AcCYP722A*. We then varied the copy numbers of *EgMAX1* and *AcCYP722A* genes. Single copies of *EgMAX1* and *AcCYP722A* made the highest titer of the CYP722A metabolite when cocultured with ECL12 (fig. S7A, YSL36). We also compared the performance of eight additional *CYP722A* orthologs in the microbial consortium and observed the highest titer with *Pisum sativum CYP722A* (*PsCYP722A*) (fig. S7B, YSL49). Coexpression of membrane steroid-binding protein 1 from *A. thaliana* (AtMSBP1) and a cytochrome P450 reductase from *Citrus sinensis* (CsCPR) further enhanced the efficiency of PsCYP722A (fig. S7, C and D, YSL58). Supplementing the growth medium with glycerol or trehalose has enhanced the performance of yeast strains that express multiple copies of cytochrome P450s (*27*), likely by stabilizing the membrane, facilitating protein folding, and enhancing regeneration of NADPH (nicotinamide adenine dinucleotide phosphate, reduced) (*28*, *29*). Likewise, we found that growing YSL58 in the presence of 2% (w/v) dextrose and 10% (v/v) glycerol during the first stage of fermentation, before coculturing with ECL12, doubled the titer of the CYP722A/B metabolite (fig. S7E). Altogether, we improved the production of the CYP722A metabolite fivefold through strain engineering and fermentation optimization (Fig. 1E).

After scaling up the fermentation of ECL12/YSL58 (table S2), we isolated sufficient CYP722A/B metabolite for structural elucidation through one-dimensional (1D) and 2D nuclear magnetic resonance (NMR) spectroscopy. Comparison of the ^{1}H NMR spectrum of the CYP722A/B metabolite to the reported ^{1}H NMR spectrum of CLA (*30*) revealed that it is a noncanonical SL, 16-hydroxy-CLA (16-OH-CLA) (Fig. 1F, fig. S8A, and table S4). This structure was further validated by using 2D ^{1}H-^{1}H–correlation spectroscopy (COSY), ^{1}H-^{13}C–heteronuclear single-quantum coherence (HSQC), ^{1}H-^{13}C–heteronuclear multiple-bond correlation (HMBC), and ^{13}C NMR spectra (fig. S8, B to E, and table S4). Circular dichroism (CD) analysis confirmed that the D-ring of 16-OH-CLA has an 11*R* configuration (fig. S9A) that is

consistent with all identified, naturally occurring SLs. Last, molecular simulations indicated that the CYP722A/B metabolite is more likely to be 16-(*S*)-OH-CLA than 16-(*R*)-OH-CLA (fig. S9C).

16-OH-CLA is widely produced by seed plants

16-OH-CLA was previously identified in *A. thaliana* as one of several oxidized derivatives of CL/CLA, but how it is made was unknown (*31*). To test whether CYP722A is required for 16-OH-CLA synthesis in vivo, we performed a metabolite analysis of *A. thaliana* plants. Although 16-OH-CLA was detected in wild type (Col-0 ecotype) and the SL-insensitive mutant *Atd14-1*, it was undetectable in the SL-deficient mutant *max3-9* and in transferred DNA (T-DNA) insertion alleles of *CYP722A*, *cyp722a-1* and *cyp722a-2* (figs. S10, S11A, S12, and S13). These observations support a role for CYP722A in 16-OH-CLA biosynthesis. Unexpectedly, 16-OH-CLA was observed only in shoot tissues, which was not the case for CLA, MeCLA, or 1′-OH-MeCLA (Fig. 2A and figs. S12 and S13). Although other SLs have been found in shoots (as well as roots or root exudates), the shoot-specific localization of 16-OH-CLA is unusual (*32*).

Consistent with the shoot-specific localization of 16-OH-CLA, we only observed *CYP722A* expression in shoot tissues (Fig. 2B and fig. S12). This contrasts with the expression of most of the other known SL biosynthesis genes in *Arabidopsis*. *CCD8/MAX4*, *CYP711A1/MAX1*, *CLAMT*, and *LBO* were expressed in both shoot and root tissues, and the latter three transcripts were enriched in roots (Fig. 2B). *CYP722A* transcript abundance increased in wild-type (WT) plants undergoing phosphate or nitrogen starvation, which is a common feature of SL biosynthesis genes in other species (*33*).

16-OH-CLA was not detectable in roots of plants that overexpress *CYP722A*, despite the use of a strong, near-constitutive *35S* promoter (Fig. 2A and fig. S12). This might be due to competition for CLA substrate, degradation or metabolism of 16-OH-CLA in roots, or export of 16-OH-CLA. Therefore, we tested whether 16-OH-CLA could be transported into shoot tissues if it were present in roots. We fed CLA and 16-OH-CLA to the roots of WT *Arabidopsis* treated with fluridone (to block SL synthesis) and *cyp722a-1* plants. Only 16-OH-CLA, and not CLA, could be detected in the shoots (fig. S15), indicating that upward and possibly selective transport of 16-OH-CLA can occur.

We then investigated whether 16-OH-CLA is made by other plants. We detected 16-OH-CLA during the initial stage of branching in poplar (*Populus nigra* × *P. grandidentata*) xylem sap (Fig. 2C and fig. S16) and in shoots of common pea (*P. sativum*) and pepper (*Capsicum annuum*) during early developmental stages (fig. S17). This compound was also detected in the shoots of the aquatic plant *Nelumbo nucifera* (fig. S17). Consistent with our observations in *Arabidopsis*, 16-OH-CLA was only detectable in shoot samples, with no trace in the corresponding roots of common pea, pepper, plum (*Prunus mume*), and *N. nucifera* (fig. S17). The levels of 16-OH-CLA gradually decreased as branching progressed and eventually phased out upon completion of branching (Fig. 2C and fig. S17). These observations indicate a dynamic regulation of 16-OH-CLA abundance during plant development that may be relevant to its physiological role.

The potentially widespread distribution of 16-OH-CLA in flowering plants was supported by testing additional *CYP722A* and *CYP722B* genes in the microbial consortium (fig. S2). 16-OH-CLA was consistently produced by CYP722A and CYP722B proteins from a diverse range of plant lineages, including gymnosperms (CjCYP722A from *Cryptomeria japonica*), early divergent angiosperms (LtCYP722A from *Liriodendron tulipifera*), eudicots (LjCYP722A from *Lotus japonicus*), and monocots (SbCYP722B from *Sorghum bicolor*) (fig. S7B and fig. S18).

To determine when 16-OH-CLA biosynthesis by CYP722A/B may have arisen in plants relative to canonical SL biosynthesis by CYP722C, we investigated the evolution of the *CYP722* family (Fig. 2D and fig. S2). Several *CYP722* representatives were previously identified in eudicot and monocot families (*34*). To supplement this, we identified 148 *CYP722* genes among 120 angiosperm and gymnosperm plant genomes and de novo transcriptome assemblies. By means of phylogenetic analysis, we found that *CYP722* likely emerged through duplication of *CYP733* in the last common ancestor of seed plants (fig. S2). Paired with the microbial consortium results, CYP722A/B proteins likely represent the original function of the CYP722 clade: 16-OH-CLA biosynthesis. The *CYP722B* clade represents a monocot-specific divergence of *CYP722A* that also produces 16-OH-CLA. The *CYP722C* clade likely emerged from *CYP722A/B* duplication in the last common ancestor of Chloranthales, Magnoliids, eudicots, and monocots. The majority (97%) of angiosperm genomes we surveyed contain at least one *CYP722* copy, although the type may vary. For example, *CYP722C* was lost in the *Brassicaceae* and *Poaceae* lineages, but

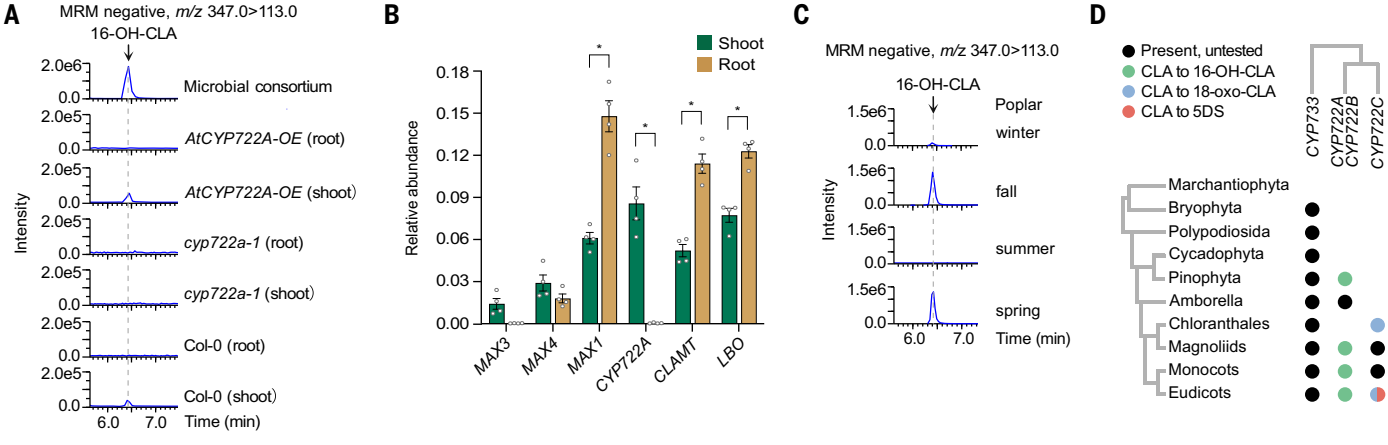

Fig. 2. Presence of 16-hydroxy-carlactonoic acid (16-OH-CLA) in plants. (**A**) Representative multiple reaction monitoring (MRM) LC-MS/MS chromatograms of 16-OH-CLA, $[M\text{-}H]^-$ *m/z* 347 > 113 in shoot or root samples of *A. thaliana* wild type and mutants in comparison with the microbial consortium. (**B**) Relative transcript abundance of SL biosynthesis genes in the shoots versus roots of hydroponically grown WT (Col-0) *A. thaliana* plants. Mean ± SEM (*n* = 4 biological replicates). Each data point indicates the average of three technical replicates. Relative expression was calculated against the housekeeping gene *CACS* by use of the Pfaffl method. *$P < 0.05$; two-way ANOVA and Šídák's multiple comparisons test. (**C**) MRM LC-MS/MS chromatograms of 16-OH-CLA in poplar (*P. nigra* × *P. grandidentata*) xylem at different seasons. (**D**) Representation map of CYP733s and CYP722 genes across major land plant clades. Black, gene copy present; green, gene copy producing 16-OH-CLA in microbial consortia present; blue, gene copy producing 18-oxo-CLA in microbial consortia present; pink, gene copy producing 5DS in microbial consortia present.

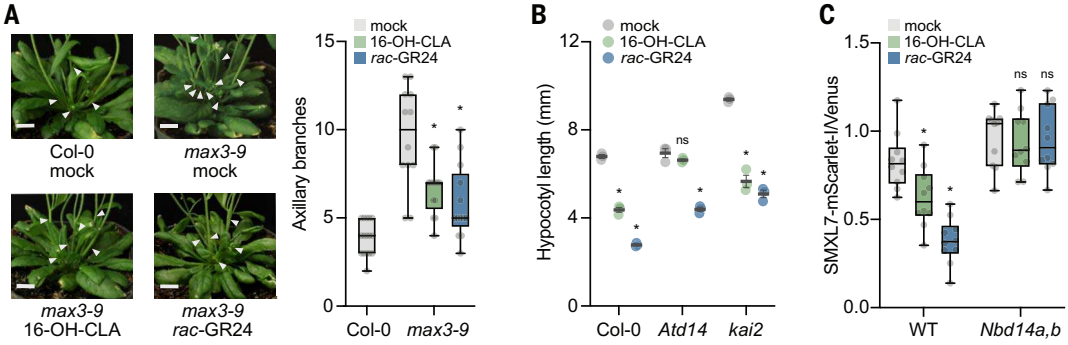

Fig. 3. 16-OH-CLA activates SL responses in planta. (**A**) 16-OH-CLA treatment suppresses axillary bud outgrowth in *max3-9* at 14 days after anthesis. Plants were treated with 0.5% (v/v) acetone, 10 μM 16-OH-CLA, or 10 μM *rac*-GR24. Boxplot whiskers indicate minimum to maximum. *P < 0.05; one-way ANOVA and Sídák's multiple comparisons test of *max3-9* mock versus treatment. Shown are representative rosette images. (**B**) 16-OH-CLA treatment inhibits *A. thaliana* hypocotyl elongation under red light through *D14*. Col-0, *d14*, and *kai2* (*htl-3* allele) seedlings were grown on media supplemented with 0.5% (v/v) acetone, 10 μM 16-OH-CLA, or 1 μM *rac*-GR24. Mean ± SEM (n = 3 replicates, mean of 17 or 18 seedlings per replicate). *P < 0.01; two-way ANOVA and Tukey multiple comparisons test of control versus treatment. (**C**) 16-OH-CLA treatment induces SMXL7 degradation through *D14*. SMXL7 ratiometric reporter was transiently expressed in WT and *Nbd14a,b N. benthamiana* leaves (n = 10). SMXL7-mScarlet-I/Venus ratios were measured after a 16- to 18-hour incubation with 0.5% (v/v) acetone, 10 μM 16-OH-CLA, or 10 μM *rac*-GR24. Each data point indicates the average fluorescence ratio of four to eight discs per leaf. Boxplot whiskers indicate minimum to maximum. *P < 0.05; two-way ANOVA and Tukey multiple comparisons test of control versus treatment.

CYP722A and *CYP722B* were retained, respectively. The prevalence of *CYP722A/B* genes, the observation of 16-OH-CLA in multiple plants, and the functional validation of CYP722A/B proteins from many plants in the microbial consortium collectively imply that 16-OH-CLA is widely present in seed plants and likely preceded the evolution of canonical SL biosynthesis by CYP722C in angiosperms.

16-OH-CLA activates SL responses in plants

To determine whether 16-OH-CLA functions as an SL, we tested its effect on the axillary shoot branching of *A. thaliana*. We used reverse-phase high-performance liquid chromatography (HPLC) to purify 16-OH-CLA made by the microbial consortium. 16-OH-CLA application inhibited the excess shoot-branching phenotype of the SL-deficient mutant *max3*, as did *rac*-GR24, which is a racemic mixture of a synthetic SL analog and its enantiomer that activates the homologous karrikin (KAR)/KAI2 ligand (KL) signaling pathway (Fig. 3A) (*35*).

We next examined the effect of 16-OH-CLA on the hypocotyl elongation of *A. thaliana* seedlings. Although endogenous SLs do not affect *A. thaliana* hypocotyl elongation, likely because of low SL abundance, application of exogenous SLs or *rac*-GR24 inhibits hypocotyl elongation under low fluence red light by inducing degradation of SMAX1 and SMXL2 (*36*, *37*). We found that 16-OH-CLA inhibited hypocotyl elongation in a manner that was dependent on the SL-receptor D14 (Fig. 3B). However, a 10-fold greater concentration of 16-OH-CLA was required to induce a degree of hypocotyl growth inhibition similar to that of *rac*-GR24 (fig. S19). As shown by the *kai2* mutant (*htl-3* allele), the stronger response to *rac*-GR24 is due to the activation of KAR/KL signaling through the receptor KAI2 in addition to SL signaling through D14, whereas 16-OH-CLA appears to signal through D14 alone (Fig. 3B).

Last, we tested whether 16-OH-CLA could induce degradation of SMXL7, an immediate consequence of D14-dependent SL signaling (*38*). We used a ratiometric reporter system to monitor the abundance of AtSMXL7 protein that was transiently expressed in *Nicotiana benthamiana* leaves (*39*, *40*). We observed that 16-OH-CLA induced degradation of the AtSMXL7 reporter in wild type but not the *Nbd14a,b* mutant (Fig. 3C). Again, 16-OH-CLA was less potent than *rac*-GR24. Because the stabilities of 16-OH-CLA and *rac*-GR24 in aqueous solutions are comparable (fig. S20), the weaker effect of 16-OH-CLA could be due to less efficient transport into plant tissues, lower affinity for D14, or a required conversion into a more bioactive metabolite. Altogether, these experiments demonstrated that 16-OH-CLA, or perhaps a downstream derivative, activates SL signaling in plants.

Functional redundancy of noncanonical SLs in *A. thaliana*

Simultaneous disruption of the noncanonical SL biosynthesis genes *CLAMT* and *LBO* has been reported to increase shoot branching of *A. thaliana*, but not as much as the CL-deficient mutant *max3* (*17*, *19*). This implies the existence of an additional, *CLAMT*/*LBO*–independent mechanism for SL biosynthesis. Therefore, we investigated whether *CYP722A* regulates shoot branching and supplements *CLAMT*/*LBO* activity.

Two *cyp722a* mutants did not show increased axillary shoot branching relative to that of wild type (figs. S11A and S21). Because 16-OH-CLA shows SL activity, there might be functional redundancy among CYP722A, CLAMT, and LBO that compensates for the 16-OH-CLA deficiency in *cyp722a*. This led us to test for synthetic enhancement among *cyp722a*, *clamt*, and *lbo* mutants. We used CRISPR-Cas9 to produce two sets of frameshift alleles for *CLAMT* and *LBO* (fig. S11, B to E) in the Col-0 background and then isolated higher-order mutant combinations with *cyp722a* T-DNA insertion alleles. Axillary branching and shoot height phenotypes were examined under nutrient-replete conditions at 14 and 28 days after anthesis. We found that *cyp722a* did not enhance *lbo* or *clamt* phenotypes (Fig. 4 and fig. S22, A to C). Unexpectedly, the branching phenotypes of the *lbo clamt* double mutants were typically as severe as the SL-deficient *max3* and SL-insensitive *d14* mutants (fig. S22, D to I). The stronger phenotype we observed for *lbo clamt* compared with the prior report could be a consequence of our growth conditions and/or a more consistent genetic background. We observed possible enhancement of *lbo-4 clamt-3* branching by *cyp722a-1* at 14 days after anthesis (fig. S22, A and J), but this did not repeat with *lbo-5 clamt-4* and *cyp722a-2* alleles (fig. S22, B, C, I, and K).

16-OH-CLA is metabolized by CLAMT and LBO

One interpretation of these results is that *CYP722A* has no role in shoot branching regulation for *A. thaliana*, at least under our nutrient-replete growth conditions. Alternatively, it may be that its product, 16-OH-CLA, is metabolized further by CLAMT and LBO into a branching regulator. In the absence of *CYP722A*, a metabolic shunt to CLA instead of 16-OH-CLA as a CLAMT substrate might produce SLs sufficient to maintain normal branching. To test the latter hypothesis, we evaluated whether 16-OH-CLA responses are dependent on *CLAMT* or *LBO* in *A. thaliana* seedlings. Hypocotyl elongation of *clamt* and *lbo* seedlings was not significantly affected by 16-OH-CLA treatment (Fig. 5A), implying that both genes are required for 16-OH-CLA bioactivity.

This led us to examine whether 16-OH-CLA can be consumed by CLAMT and LBO. We

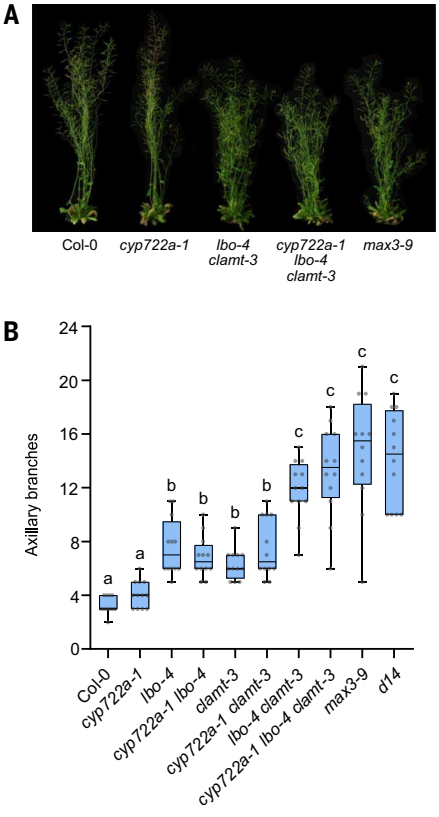

Fig. 4. Functional redundancy in branching inhibition by noncanonical SLs in *A. thaliana*. (**A**) Composite image of representative Col-0, *cyp722a-1*, *lbo-4 clamt-3*, *cyp722a-1 lbo-4 clamt-3*, and *max3-9* plants at 28 days after anthesis. (**B**) Rosette axillary branches (>6 mm) at 28 days after anthesis. Boxplot whiskers indicate minimum to maximum. *P < 0.05; Brown-Forsythe and Welch ANOVA and Dunnett's multiple comparisons test.

introduced *AtCLAMT* into the CLA-producing and 16-OH-CLA–producing consortia (ECL12/YSL22 and ECL12/YSL55) (table S2), generating ECL12/YSL61 and ECL12/YSL65, respectively. Peaks consistent with the identity of MeCLA (RT at 19.72 min, positive ion at m/z 347.1) (*31*) and methyl 16-hydroxycarlactonoate (16-OH-MeCLA) (RT at 14.64 min, positive ion at m/z 363.1) were detected in ECL12/YSL61 and ECL12/YSL65, respectively, but not in the negative control consortia ECL12/YSL59 and ECL12/YSL63 that lack CLAMT (figs. S23 to S25 and table S2). The conversion of CLA to MeCLA and 16-OH-CLA to 16-OH-MeCLA by AtCLAMT was highly efficient. We obtained similar results in microbial consortia expressing *CLAMT* variants from several eudicot species (fig. S26), suggesting that CLAMT activity on CLA and 16-OH-CLA is conserved. We then used yeast whole-cell biotransformation assays, in which different substrates were supplied to yeast cells expressing *AtCLAMT* or *CYP722A* alone (as described in section "Yeast-based whole-cell biotransformation assay"), to elucidate the steps of 16-OH-MeCLA formation from CLA. These assays showed that AtCLAMT converts 16-OH-CLA into 16-OH-MeCLA, but CYP722A does not convert MeCLA into 16-OH-MeCLA (fig. S27). Therefore, CYP722A acts upstream of CLAMT.

In contrast to CLAMT, LBO did not metabolize CLA or 16-OH-CLA in microbial consortia (figs. S23 and S24 and table S2). We then introduced *LBO* and *CLAMT* together into CLA and 16-OH-CLA–producing consortia (ECL12/YSL22 and ECL12/YSL55) (table S2), generating ECL12/YSL62 and ECL12/YSL66, respectively. Consistent with prior studies of LBO and MeCLA, a peak likely to be 1′-OH-MeCLA (RT at 14.13 min, positive ion at m/z 363.1) was detected in both ECL12/YSL62 and ECL12/YSL66 (figs. S23 and S24) (*17*, *31*). There also was a decrease in the abundance of 16-OH-MeCLA in ECL12/YSL66 in comparison with ECL12/YSL65 (fig. S24 and table S2), which might be due to LBO shunting CLA metabolism to 1′-OH-MeCLA or the conversion of 16-OH-MeCLA by LBO to a downstream product. To examine whether LBO can act on 16-OH-MeCLA, we fed 16-OH-CLA to yeast cells coexpressing *AtCLAMT* and *AtLBO*. Almost all 16-OH-CLA was consumed, but little 16-OH-MeCLA was observed compared with yeast that only expressed *AtCLAMT* (Fig. 5B and fig. S28). This suggests that LBO can metabolize 16-OH-MeCLA efficiently. This is also consistent with our observation of 16-OH-MeCLA accumulation in the *lbo* mutant (fig. S10). However, the exact identity of its product remains unknown (fig. S28).

We then examined whether 16-OH-MeCLA is normally produced in plants. Similar to 16-OH-CLA, 16-OH-MeCLA was observed only in the shoot tissues of Col-0 and *Atd14* plants but not the *cyp722a* mutants (Fig. 5C and figs. S10 and S12). 16-OH-MeCLA was also observed in poplar, pea, pepper, and *N. nucifera*, exhibiting a pattern of abundance during development that was similar to that of 16-OH-CLA (Fig. 5D and figs. S16 and S17). In a sample of plum (*P. mume*) shoot tissues collected at the onset of budding, 16-OH-MeCLA was observed, but 16-OH-CLA was not (fig. S17). These findings suggest that CLAMT, potentially with the subsequent activity of LBO, converts 16-OH-CLA into additional SLs that might regulate shoot branching (Fig. 5E).

Evolution of 18-OH-CLA biosynthesis in the CYP722 clade

We propose that *CYP722C* evolved from duplication and neofunctionalization of *CYP722A* within the angiosperm lineage. The critical difference between CYP722A and CYP722C activity on CLA substrate is the oxidation of C16 versus C18 on the A-ring, respectively. Putatively, this difference could have evolved through a mutation (or mutations) in the CYP722A active site that causes the A-ring of CLA to rotate ~180°, placing C18 instead of C16 near the site of oxidation.

To investigate this hypothesis, we conducted molecular docking analysis of CLA with AlphaFold2 models (*41*) of a CYP722A protein from a gymnosperm, *Cryptomeria japonica*, and a CYP722C protein from a legume, *Lotus japonicus* (Fig. 5F and fig. S29). CjCYP722A and LjCYP722C1 are predicted to share a similar structural fold common to cytochrome P450s, featuring a triangular prism shape with a heme group buried in the center and stabilized by a cysteine residue (fig. S29, A and B). Despite their close structural similarity, there are substantial sequence differences within the substrate-binding cavity that may account for their ability to catalyze oxidation of CLA at different positions. By comparing these models and analyzing sequence conservation among CYP722A/B and CYP722C proteins, we identified eight amino acid residues in CjCYP722A (V74, T119, A356, S357, S360, H464, F465, and P466) that may impact the oxidation site of CLA. (Single-letter abbreviations for the amino acid residues are as follows: A, Ala; F, Phe; H, His; I, Ile; P, Pro; S, Ser; T, Thr; and V, Val.)

We used the microbial consortium to test single and higher-order substitutions of six residues in CjCYP722A with CYP722C identities (fig. S30). A single amino acid substitution, F465I (in which phenylalanine was replaced at position 465 with isoleucine), was sufficient for CjCYP722A to gain 18-OH-CLA production (Fig. 5F). Equivalent substitutions in CYP722A proteins from *Liriodendron tulipifera* (Magnoliids), *L. japonicus*, and *P. sativum* also led to 18-OH-CLA production (fig. S30). A reverse substitution in LjCYP722C1, I472F, did not give rise to 16-OH-CLA synthesis, however. These mutations of CYP722A proteins were often associated with reduced activity, and 16-OH-CLA synthesis remained (fig. S30). Therefore, these observations demonstrate that 18-OH-CLA synthesis could have evolved easily in a CYP722A paralog, but additional mutations must have been critical during the neofunctionalization process that led to CYP722C.

Discussion

We showed that proteins from the CYP722A clade and its sister group in monocots, CYP722B, carry out the synthesis of a noncanonical SL, 16-OH-CLA. 16-OH-CLA is present at very low concentrations, with variation in space and time in plants; at least 300 liters of xylem sap from poplar is required to isolate enough compound for NMR analysis (fig. S31). By engineering a microbial consortium that produces SLs heterologously, we can now synthesize >1 mg of 16-OH-CLA from a 5-liter culture within 6 days. Putatively, this system could be used to produce many SLs for physiological and biochemical studies that are otherwise inaccessible owing to the difficulty and cost of organic synthesis or

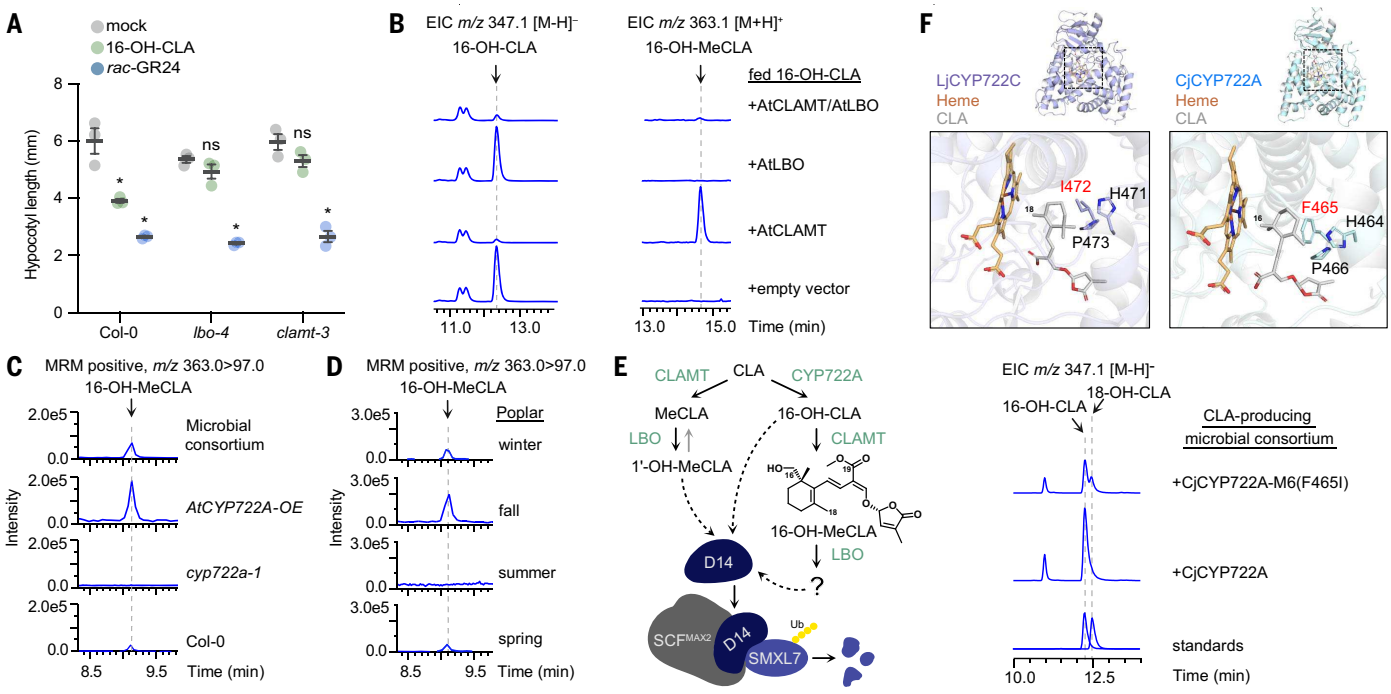

Fig. 5. The function of 16-OH-CLA is CLAMT- and LBO-dependent. (**A**) 16-OH-CLA treatment inhibits *A. thaliana* hypocotyl elongation under red light through *LBO* and *CLAMT*. Col-0, *lbo-4*, and *clamt-3* seedlings grown on media supplemented with 0.5% (v/v) acetone, 10 μM 16-OH-CLA, or 1 μM *rac*-GR24. Mean ± SEM (n = 3 replicates, mean of 17 or 18 seedlings per replicate). *P < 0.01; two-way ANOVA and Tukey multiple comparisons test of control versus treatment. (**B**) Yeast whole-cell biotransformation assay by using purified 16-OH-CLA as the substrate. LC-MS EIC SIM at 16-OH-CLA and 16-OH-MeCLA characteristic ions $[M\text{-}H]^-$ = 347.1 and $[M+H]^+$ = 363.1, respectively, of yeast strains expressing CLAMT and/or LBO, with yeast containing an empty vector as a negative control. (**C** and **D**) MRM LC-MS/MS of 16-OH-MeCLA, $[M+H]^+ m/z$ 363 > 97 in (C) shoots of *A. thaliana* wild type and mutants and (D) poplar xylem at different seasons. (**E**) Proposed model of noncanonical SL biosynthesis by *CYP722A*, *CLAMT*, and *LBO*. Multiple noncanonical SLs might activate D14 (dashed lines). (**F**) Single mutation in CYP722A conferring 18-oxidation activity on CLA. (Top) Key residues in the CLA-docking models of LjCYP722C1 and CjCYP722A. (Bottom) LC-MS EIC SIM at $[M\text{-}H]^-$ = 347.1 of ECL12 cocultured with YSL22 expressing CjCYP722A or CjCYP722A-M6 ($CjCYP722A^{F465I}$) (figs. S29 and S30).

purification from plants. The microbial consortium also enabled us to rapidly characterize many CYP722A/B proteins as well as CYP722 active-site mutants, highlighting the benefits of using microbial cell factories to study secondary metabolism in plants.

The physiological role of 16-OH-CLA remains enigmatic. So far, 16-OH-CLA is the only SL that has been found exclusively in aboveground tissues. Its abundance varies across seasons and developmental stages, but what purpose this serves is not yet clear. We found that 16-OH-CLA shows several SL activities, including inhibition of axillary branching and triggering SMXL7 degradation. However, in seedlings, 16-OH-CLA activity was mostly dependent on CLAMT and LBO, which together can form 16-OH-MeCLA and putatively an additional unknown metabolite (Fig. 5E). One or more of these downstream metabolites may be a better agonist of D14 than 16-OH-CLA itself. Unexpectedly, the absence of 16-OH-CLA had no effect on branching in *Arabidopsis*, suggesting that SL signaling was intact. Putatively, this is because CLAMT and LBO can also synthesize alternative noncanonical SLs, MeCLA, and 1′-OH-MeCLA from CLA directly. It seems likely that multiple noncanonical SLs may function as hormones. It will be important to determine their relative activities and abundance in plants to understand their individual contributions to hormone signaling.

We found that a single mutation in CYP722A, F465I, is sufficient to gain production of 18-OH-CLA (Fig. 5F and fig. S30). This suggests a likely origin for an important biosynthetic precursor of canonical SLs in angiosperms. CYP722C is not the only route to canonical SL formation in angiosperms; specialized CYP711A/MAX1 paralogs perform this role in some species (*15*, *16*). However, the *CYP722C* family is broadly distributed in angiosperms, and its members have consistently shown canonical SL biosynthesis activity (*7*, *20*–*22*). In comparison, observations of *CYP711A* diversification giving rise to canonical SL biosynthesis have been relatively infrequent; most CYP711A proteins tested so far appear to produce CLA (*15*, *16*). This suggests that CYP722C has a predominant role in canonical SL biosynthesis in angiosperms, which is not the case in other plants. Canonical SLs have been reported in *Selaginella moellendorffii* (a lycophyte) and three gymnosperms, which lack *CYP722C* (*42*). Therefore, a *CYP722C*-independent mechanism (or mechanisms) for canonical SL biosynthesis exists outside of the angiosperms. In *S. moellendorffi*, at least, this is putatively due to *CYP711A* diversification (*43*).

Canonical SLs have important roles in plant biotic interactions in angiosperms. However, the evolution of canonical SLs was not strictly necessary for the establishment of interorganismal communication in soil. For example, the bryophyte *Marchantia paleacea* uses a noncanonical SL, bryosymbiol, for recruitment of AM fungal symbiosis but not as a hormone (*44*). Perhaps the adoption of SLs as hormones, greater chemical stability or mobility of canonical SLs in soil, or ongoing coevolution between plants and symbionts drove the division of noncanonical and canonical SLs into internal and external roles in flowering plants, respectively.

Materials and methods

Chemicals and general culture conditions

(±)5-deoxystrigol (5DS) (purity >98%) and (±)-orobanchol (ORO) were purchased from Strigolab (Italy). *rac*-GR24 was from Phyto-Tech Labs. The chemically competent *E. coli* strain TOP10 (Life Technologies) was used for DNA manipulation and amplification. All

engineered *E. coli* strains for protein expression and CL production in this work are listed in table S2 and constructed in *E. coli* strain BL21(DE3) (Novagen). *E. coli* strains were grown at 37°C in Luria-Bertani (LB) medium (Fisher Scientific) supplemented with appropriate amount of antibiotics (100 μg/ml ampicillin (Fisher Scientific), 50 μg/ml kanamycin (Fisher Scientific), 25 μg/ml chloramphenicol (Fisher Scientific), and 50 μg/ml spectinomycin (Sigma-Aldrich) for plasmid maintenance.

All engineered *S. cerevisiae* strains for SL production in this work are listed in table S2 and constructed in a haploid CEN.PK2.1D background (*MATα*; *his3D;1 leu2–3_112; ura3–52; trp1–289; MAL2–8c; SUC2*). Yeast strains were cultured at 30°C in synthetic defined (SD) medium containing yeast nitrogen base (YNB) (BD Diagnostics), ammonium sulfate (Fisher Scientific), 2% (w/v) dextrose (unless specified) and the appropriate dropout (Takara Bio) solution for selection.

E. coli-S. cerevisiae consortium was co-cultured in XY medium, which contains 13.3 g/liter KH_2PO_4, 4 g/liter $(NH_4)_2HPO_4$, 1.7 g/liter citric acid, 0.0025 g/liter $CoCl_2$, 0.015 g/liter $MnCl_2$, 0.0015 g/liter $CuCl_2$, 0.003 g/liter H_3BO_3, 0.0025 g/liter Na_2MoO_4, 0.008 g/liter $Zn(CH_3COO)_2$, 0.06 g/liter $FeSO_4$, 0.0045 g/liter thiamine, 1.3 g/liter $MgSO_4$, 5 g/liter yeast extract, and 40 g/liter xylose, pH 7.0. Unless specified, all the chemicals used in this study were purchased from Fisher Scientific or Sigma-Aldrich Co.

General techniques for DNA manipulation

Plasmid DNA was prepared using the Econospin columns (Epoch Life Science) according to manufacturer's protocols. Polymerase chain reaction (PCR) was performed using the Expand High Fidelity PCR System (Roche Life Science) according to the manufacturer's protocols. PCR products were purified by Zymoclean Gel DNA Recovery Kit (Zymo Research). All DNA constructs were confirmed through DNA sequencing by Genewiz (San Diego, CA, United States). *E. coli* expression plasmids were constructed via Gibson cloning method (*45*). Restriction enzymes (NEB) and T4 ligase (NEB) were used to produce and ligate the DNA fragments, respectively. Gibson one-pot, isothermal DNA assembly was conducted at 10 μl scale by incubating T5 exonuclease (NEB), Phusion polymerase (NEB), Taq ligase (NEB) and 50 ng of each DNA fragment at 50°C for 1 hour to assemble multiple DNA fragments into one circular plasmid. BP Clonase II Enzyme Mix, Gateway *pDONR221* Vector and LR Clonase II Enzyme Mix (Invitrogen) and the *S. cerevisiae* Advanced Gateway Destination Vector Kit (Addgene) were used to perform Gateway Cloning for construction of the yeast expression plasmids. Plasmid-harboring yeasts were constructed using the lithium acetate transformation method. Integrated yeast strains were constructed through homologous recombination and DNA assembly. Plasmids utilized in this study are listed in table S1. DNA oligonucleotides and genes were synthesized by Integrated DNA Technologies (IDT, Coralville, IA, United States). All variants of *D27*, *CCD7* and *CCD8* expressed in *E. coli* and all genes expressed in *S. cerevisiae* (such as CYP genes) were codon-optimized by GenScript Biotech (Piscataway, NJ, United States). DNA sequences of genes involved in this work are listed in table S7.

Site-directed mutagenesis

To generate the mutants of CjCYP722A, LtCYP722A, LjCYP722A, PsCYP722A, and LjCYP722C1, a pair of complementary primers containing the desired mutations was designed to amplify the destination vector *pAG414GPD* harboring the corresponding gene. PCR was performed using Q5 High-Fidelity DNA Polymerase (NEB). The parental plasmid DNA was digested with DpnI for 1 hour at 37°C, and the PCR product was purified and transformed into competent *E. coli* cells via heat-shock transformation. Colonies were screened by sequencing to confirm the presence of the desired mutation. In vivo functional validation of the mutants was carried out as described in sections "Culture conditions for *E. coli–S. cerevisiae* consortium-based SL production" and "Isolation and analysis of SLs and SL precursors from microbial consortia."

Culture conditions for E. coli–S. cerevisiae consortium-based SL production

For the in vivo production of SLs or the functional identification of new biosynthetic enzymes, *E. coli-S. cerevisiae* consortium was performed in a 2-stage fermentation. In the first stage of fermentation, a single colony of an engineered *E. coli* strain for CL production (ECL#) was picked and grown overnight at 37°C and 220 revolutions per minute (rpm) in 0.5 ml of LB supplemented with appropriate amounts of corresponding antibiotics. The overnight culture was 1% inoculated into 1 ml of fresh LB with the corresponding antibiotics with a starting OD_{600} (optical density of a sample measured at a wavelength of 600 nm) at ~0.05 and cultured at 37°C and 220 rpm in the 15 ml glass tube. When OD_{600} reached ~0.6, IPTG was added into the medium with a final concentration of 0.5 mM (unless specified) to induce the gene expression. Then the culture was incubated at 18°C and 220 rpm for 16 to 18 hours. In parallel to preparing the *E. coli* culture, a single colony of an engineered Yeast strain for SL production (YSL#) was picked and grown overnight at 30°C and 220 rpm in the corresponding SD medium based on the auxotrophic markers for maintaining the plasmid(s). The overnight seed culture was 2% incubated into 1 ml of fresh corresponding SD medium or SD medium supplementing with additional glycerol or trehalose in a 15 ml glass tube and grown at 30°C for 16-18 hours.

In the second stage of fermentation, the *E. coli* and yeast cells prepared as described above were harvested by centrifugation at 3500 rpm for 3 min, following by being mixed and resuspended in 1 ml of XY media (OD_{600} ~ 8.0) and co-cultured in 15 ml glass tubes at 25°C and 220 rpm for 48 hours (final OD_{600} ~ 40).

Isolation and analysis of SLs and SL precursors from microbial consortia

Unless specified, 1 ml culture was used for compound extraction. For the extraction of intracellular and extracellular metabolites, 1 ml of co-culture was transferred into a 15 ml centrifuge tube and added 0.5 ml of disruption zirconis/sillica beads for *E. coli* and yeast (RPI), and resuspended in 1 ml of ethyl acetate and vigorous shaking for 5 min by using a homogenizer (FastPrep-24 Classic), and centrifugation at 5000 rpm for 10 min. Then the upper ethyl acetate layer was transferred into a 1.7 ml microcentrifuge tube and evaporated to dryness in a vacuum concentrator (Eppendorf vacufuge plus, Enfifield, CT, United States) at room temperature for 30 min. The dried extract was redissolved in 60 μl of acetone and centrifuged at 12,000 rpm for 10 min. 10 μl of each sample was applied to liquid chromatography-mass spectrometry (LC-MS) (Shimadzu LC-MS 2020 (Kyoto, Japan)). Both ultraviolet visible (UV-vis) and mass spectrometry (MS) detectors were used.

All the SL precursors and SLs were analyzed using a reverse phase (RP) column (Kinetex C18, 100 mm × 2.1 mm, 100Å, particle size 2.6 μm; Phenomex, Torrance, CA, United States). LC-MS parameters: column temperature 40°C; mobile phase A: 0.1% (v/v) formic acid in water; mobile phase B: 0.1% (v/v) formic acid in acetonitrile (MeCN); gradient elution at 0.4 ml/min. The gradient was as follows: 0 to 28 min, 5 to 100% B; 28 to 35 min, 100% B; 35 to 40 min, 5% B. The UV-vis absorption was monitored in the range of 190 to 800 nm. The compounds without wavelength information were detected using an MS detector, which operates in the mass/charge ratio (m/z) range of 50–800 in the positive or negative ion modes. Electrospray Ionization (ESI) was used. The desolvation line temperature was 250°C. The nebulizing gas and drying gas flow rates were 1.5 liter/min and 15 liter/min, respectively. The RT and the characteristic m/z or absorption wavelength of various analytes are listed as follows: carlactone (CL), 21.04 min (positive ion at m/z 303.2 or 269 nm); carlactonoic acid (CLA), 16.81 min (negative ion at m/z 331.1); methyl carlactonoate (MeCLA), 19.72 min (positive ion at m/z 347.1); 18-hydroxy carlactonoic acid (18-OH-CLA), 12.54 min (negative ion at m/z 347.1); 16-hydroxy carlactonoic acid (16-OH-CLA), 12.32 min (negative ion at m/z 347.1); methyl 16-hydroxy carlactonoate (16-OH-MeCLA),

14.64 min (positive ion at *m/z* 363.1); hydroxymethyl carlactonoate (1′-OH-MeCLA), 14.13 min (positive ion at *m/z* 363.1); 5DS, 16.38 min, (positive ion at *m/z* 331.1); ORO, 11.41 min, (positive ion at *m/z* 347.1); *rac*-GR24, 12.03 min, (positive ion at *m/z* 299.1).

Purification and structural elucidation of 16-OH-CLA

To obtain a sufficient amount of 16-OH-CLA for structural elucidation by NMR, 1 ml of the 2-stage fermentation described above was scaled up to 400 ml culturing in a 2-liter shake flask at 25°C for 48 hours. The yeast culture medium was separated from cell pellets by centrifugation at 5000 rpm for 20 min. The supernatant was extracted with an equal amount of ethyl acetate. The cell pellet was extracted with 100 ml of acetone. The resultant organic extracts were combined and evaporated to dryness using Rotavapor R-100 (BUCHI), then redissolved in ethyl acetate. 16-OH-CLA was purified by reverse-phase HPLC (C18, 5 mm, 250 10 mm, Phenomex, Torrance, CA, United States) using the same method as LC-MS analysis. The ^{1}H, ^{13}C, ^{1}H–^{1}H correlation (COSY), heteronuclear multiple quantum coherence (HMQC) and heteronuclear multiple bond correlation (HMBC) NMR spectra were recorded on the Bruker Avance III 700 spectrometer operating at 700MHz using C_6D_6 as the solvent.

NMR data of 16-OH-CLA were as follows: ^{1}H-NMR (700 MHz, C_6D_6): 7.64 (1H, s, H-10), 7.13 (1H, d, J = 16.94 Hz, H-7), 6.48 (1H, d, J = 16.52 Hz, H-8), 5.77 (1H, s, H-12), 5.14 (1H, s, H-11), 3.64 (1H, d, J = 10.84 Hz, H-16), 3.35 (1H, d, J = 10.83 Hz, H-16), 1.85, 1.91 (2H, m, H-4), 1.80 (3H, s, H-18), 1.52-1.57 (2H, m, H-3), 1.34 (3H, s, H-15), 1.26-1.29 (2H, m, H-2), 1.06 (3H, s, H-17); ^{13}C-NMR (700 MHz, C_6D_6) δ: 10.22, 19.25, 22.02, 23.40, 32.87, 33.63, 40.11, 70.14, 100.61, 112.24, 122.65, 132.85, 133.12, 135.17, 135.37, 140.74, 154.09, 169.90, 171.64.

Evaluation of the stability of 16-OH-CLA and rac-GR24

Two mM stock solutions of 16-OH-CLA and *rac*-GR24 were diluted with distilled (DI) water (pH 8.5) into 10 μM working solutions which were incubated at a static state at 25°C for 14 days. 10 μl of each solution containing 10 μM 16-OH-CLA and *rac*-GR24 were collected at different time points (0.5, 1, 3, 7, and 14 days) and analyzed by LC-MS using the same method as mentioned in section "Isolation and analysis of SLs and SL precursors from microbial consortia." The peak area of 16-OH-CLA's characteristic negative ion at *m/z* 347.1 and *rac*-GR24's characteristic positive ion at *m/z* 299.1 were used to calculate the amount of compounds left.

Yeast-based whole-cell biotransformation assay

The *ATR1*-integrated yeast strain (YSL20) expressing *AtCLAMT* (YSL68/YSL83), *AtLBO* (YSL84), *AtCLAMT* and *AtLBO* (YSL85), and *PsCYP722A* (YSL69) were used for the whole-cell biotransformation assay. The *ATR1*-integrated yeast strain (YSL20) harboring empty vector(s) (YSL67/YSL82) were used as negative controls. Taking YSL67 as an example, a fresh yeast colony was first inoculated into 1 ml of SD medium and cultured overnight at 30°C and 220 rpm. 20 μl of the overnight culture was used to inoculate into 1 ml of fresh SD medium in a test tube and grown at 30°C with shaking at 220 rpm for 18 hours. The cells were then harvested by centrifugation at 3000 rpm and resuspended in 1 ml of SD medium. 16-OH-CLA, CLA crude extract, and MeCLA crude extract were separately fed to 1 ml of YSL67 biotransformation matrix at a final concentration of approximately 0.08 mg/liter, incubated at 25°C, and 220 rpm for 12 hours. The reaction mixture was quenched by adding an equal volume of ethyl acetate followed by vigorous vortexing. The quenched reaction mixtures were then centrifuged at 13,000 rpm for 10 min. The ethyl acetate phase was then collected and concentrated in a vacuum concentrator. The residue was redissolved in 50 μl of acetone. The solution was centrifuged at 13,000 rpm for 10 min, then 10 μl of samples were subjected to LC-MS analysis as described above.

Crude extracts of CLA and MeCLA were extracted from 50 ml of ECL12/YSL24 and ECL12/YSL61 respectively, using a similar method as described above in section "Isolation and analysis of SLs and SL precursors from microbial consortia."

Isolation and characterization of SLs and SL precursors from plants

Each plant was grown in a greenhouse maintained at 22° to 28°C under natural daylight conditions. Each part of the plant was harvested and extracted with ethyl acetate for at least 3 days, and crude extracts were purified by silica Sep-pack cartridge as reported previously (*46*). For poplar, a hole was made in the trunk of a poplar (*P. nigra* × *P. grandidentata*) tree 30 cm from the ground, a vacuum pump was connected to the hole, and the duct fluid was collected by suctioning at −0.08 MPa for 4 to 8 hours a day for a week (fig. S31). The collected xylem sap was extracted with ethyl acetate to obtain crude extracts after concentration.

SLs extracted from plants were analyzed using LC-MS/MS with product ion scan (PIS) and multiple reaction monitoring (MRM) as reported previously (*31*). Each molecule was identified through at least two ion transitions (table S8). Briefly, analysis was performed with a QTRAP5500 (AB Sciex) equipped with an electrospray source and UPLC (Nexera X2; Shimadzu) using a RP column (Kinetex C18, 2.1 by 150 mm, 1.7 μm; Phenomenex). A linear gradient from 35 to 95% acetonitrile over 19 min was applied, with the column oven maintained at 30°C.

Plant materials

Arabidopsis thaliana alleles in the Col-0 ecotype used in this study were *d14-1*, *kai2* (*htl-3* allele), and *max3-9* (*47*–*49*). The *cyp722a-1* (SALK_088395) and *cyp722a-2* (SALK_059996) alleles were obtained from The Salk Institute Genomic Analysis Laboratory (*50*). The *N. benthamiana Nbd14a,b* allele used in this study was described previously (*39*).

Generation and genotyping of Arabidopsis *mutant lines*

Two *LBO* (At3g21420) sites 5′-CACCGCTAATCGAAGAAATAGGTAGAGG-3′ and 5′-CACCGGCATAGGGCAGTAACAAACAGGG-3′ (protospacer adjacent motif underlined), were selected using CRISPR-P v2.0 (*51*). Both gRNA sequences were introduced into *pYUU* (*52*) using GoldenGate cloning and Q5 DNA Polymerase (New England Biolabs) for gRNA cassette amplification (*53*). *pYUU-lbov4* was verified by Sanger sequencing. *cyp722a-1* was transformed by floral dip method (*54*) and the T1 seeds were screened for seed coat-YFP fluorescence with a (~470 nm) blue LED flashlight and orange safety glasses. The *lbo-4* allele [1 base pair (bp) insertion between +12 and +13 in the coding sequence] was identified by Sanger sequencing.

Two *CLAMT* (At4g36470) sites 5′-CTCTTTTGATCTACACCGGAGG-3′ and 5′-CAGCTTTATATGACGAGCAAGG-3′ (protospacer adjacent motif underlined), were selected using CRISPR-P v2.0. Both gRNA sequences were introduced into *pYUU* and the wildtype Col-0 was transformed as described above. *pYUU-clamtv3* was verified by Sanger sequencing. The *clamt-3* allele (1 bp insertion between +632 and +633 in the coding sequence) was identified by Sanger sequencing. *cyp722a-1 lbo-4* was crossed to the *clamt-3* plant and transgene-free F1 seeds were selected by screening with (~470 nm) blue light. Homozygous single, double, and triple mutants were identified in the F2 generation by PCR verification. Additionally, PCR with 5′-TGTCCCAGGATTAGAATGATTAGGC-3′ (U6-26p-F) and 5′-AGCCCTCTTCTTTCGAT CCATCAAC-3′ (U6-29p-R) was performed to confirm transgene-free F2 seeds (*53*).

Two *LBO* (At3g21420) sites 5′-GATCAGGACTTGAACATGGAGGG-3′ and 5′-GGACTTAGTCCACATTCTGATGG-3′ (protospacer adjacent motif underlined), were selected using CRISPR-P v2.0 (*51*). Both gRNA sequences were introduced into *pYUU* (*52*) using GoldenGate cloning and Q5 DNA Polymerase (New England Biolabs) for gRNA cassette amplification (*53*). *pYUU-lbov5* was verified by Sanger sequencing. *cyp722a-2* was transformed by floral dip method (*54*) and the T1 seeds were screened for seed coat-YFP fluorescence with a (~470 nm) blue LED flashlight and orange safety glasses. The *lbo-5*

allele (5 bp deletion between +665 and +671 and 1 bp insertion between +707 and +708 in the coding sequence) was identified by Sanger sequencing.

Two *CLAMT* (At4g36470) sites 5′-TCTTCCATAAAATGACCCAGGG-3′ and 5′-CGGTGGTGAGCAACTTGGACGG-3′ (protospacer adjacent motif underlined), were selected using CRISPR-P v2.0. Both gRNA sequences were introduced into *pYUU* and the WT Col-0 was transformed as described above. *pYUU-clamtv4* was verified by Sanger sequencing. The *clamt-4* allele (1 bp deletion between +238 and +240 and 20 bp deletion between +400 and +421 in the coding sequence) was identified by Sanger sequencing. *cyp722a-2 lbo-5* was crossed to the *clamt-4* plant and transgene-free F1 seeds were selected by screening with (~470nm) blue light. Additionally, PCR with 5′-TGTCCCAGGATTAGAATGATTAGGC-3′ (U6-26p-F) and 5′-AGCCCTCTTCTTTCGATCCATCAAC-3′ (U6-29p-R) was performed to confirm transgene-free F2 seeds (*53*). The *lbo-5 clamt-4 and lbo-5 clamt-4 cyp722a-2* alleles were identified in the F2 generation by PCR and sequence verification.

Both *cyp722a* alleles were genotyped using 5′-TTGTATAGCCAGCCTCGATTG-3′ (RP), 5′-AAATTGAGAGGAAAAGCGAGC-3′ (LP), and a T-DNA left border-specific primer 5′-ATTTTGCCGATTTCGGAAC-3′ (LB3.1). Primers were selected using T-DNA Express. The PCR products were run on a 1.2% RA-agarose gel. The alleles can be differentiated by their mutant PCR (RP + LP) product size. *cyp722a-1* (~600 bp) and *cyp722a-2* (~700 bp). The *lbo-4* allele was identified using PCR by 5′-CTTTCTTGGTCTGCTTTCAATATGGCTCCTgTA-3′ and 5′-TGAAGATGATGAGTCTTAAGAGACGACACAAC-3′ (mismatch for dCAPS marker in lowercase). dCAPs primers were selected using indCAPS (*55*). The PCR products were digested with RsaI-HF (New England Biolabs) and run on a 3% LE-agarose gel. The *lbo-5* allele was identified using PCR by 5′-GTGAAAGTCTTGAAGGTTACTC-3′ and 5′-CATTGGGAAGAGGTTTAACAGG-3′. The PCR products were digested using NlaIII (New England Biolabs) and run on a 3% LE-agarose gel. The *clamt-3* allele was identified using PCR by 5′-GGAAGATTTCTCCATTTTCCTaCG-3′ and 5′-CTTGAGAGAAGTTCCCAAAAGAA AGAG-3′ (mismatch for dCAPS marker in lowercase). The PCR products were digested with MluI-HF (New England Biolabs) and run on a 3% LE-agarose gel. The *clamt-4* allele was identified using PCR by 5′-CTCTCTCCACCATTACAGACTTCATC-3′ and 5′-GAGAGGCATAGACAAAGTGGATGG-3′. The PCR products were run on a 3% LE-agarose gel.

Generation and genotyping of A. thaliana CYP722A-OE lines

AtCYP722A isoform 1 (TAIR) was yeast-codon optimized and synthesized by Twist Bioscience with attB Gateway cloning sites. *AtCYP722A.1* was cloned into a pGWB402 (*56*) vector modified with a YFP selectable marker from pYUU (*52*) (*pGWBcitr-p35S* destination vector) and verified by Sanger sequencing. Col-0 was transformed by floral dip method (*54*) and T1 seeds were screened for seed coat-YFP fluorescence with a (~470 nm) blue flashlight. Transgenic lines were verified by genotyping using primers 5′-GAAGTTGTGGACGAGGACC-3′ (*AtCYP722A*-specific) and 5′-AAGACCGGCAACAGGATTC-3′ (vector-specific).

Plant propagation and transformation

Plants were propagated in Sungro Professional Growing Mix under white light (~110 umol m^{-2} s^{-1}; MaxLite LED T8 16.5W 4000K light-emitting diode bulbs) with 16 hours light/8 hours dark photoperiod at ~21° to 24°C. Soil was supplemented with Gnatrol WDG, Marathon (imidacloprid), and Osmocote 14-14-14 fertilizer. Seeds were frozen at −80°C for 24 hours and then surface-sterilized. Sterilization was performed by agitating for 5 min in a 0.05% (v/v) Triton X-100, 70% EtOH solution, washing 1× with 70% EtOH and 1× with 95% EtOH, and air-drying. Seeds were grown on 0.5× Murashige-Skoog (MS) medium with 0.8% Sigma Aldrich Agar (pH 5.8), unless otherwise specified. Floral dip transformation of *A. thaliana* with *Agrobacterium tumefaciens* (GV3101 pMP90) was performed in 5% sucrose (w/v) and 0.05% (v/v) Silwet-77 (*54*).

SL identification and quantification in Arabidopsis

For soil-grown plants, *A. thaliana* seeds were surface-sterilized in 70% ethanol containing 0.01% Tween 20 for 5 min, followed by rinsing with sterile water. The seeds were then imbibed in sterile, distilled 0.1% agarose at 4°C for 3 days before being sown directly onto autoclaved potting mix soils [horticultural soil: vermiculite = 1:2 (v/v)]. The plants were grown under controlled conditions with a 16-hour light/8-hour dark cycle at 22°C. The basal parts of the shoot and root tissues were harvested, and the metabolites were extracted with ethyl acetate for 4 days at 8°C. The crude extracts were subsequently purified by DEA and silica cartridge.

Quantitative analysis of SLs, including CLA, MeCLA, 1′-OH-MeCLA, 16-OH-CLA, and 16-OH-MeCLA, were performed using the same MRM analysis on LC-MS/MS as aforementioned in section "Isolation and characterization of SLs and SL precursors from plants." The quantification of SLs was conducted using both natural and synthetic standards. Extract samples were dissolved in 50% aqueous MeCN. An aliquot of the filtered 50% aqueous MeCN sample solutions was diluted with either pure 50% MeCN or 50% MeCN containing known amounts of SLs. The increase in peak area on the chromatogram corresponded to the amounts of each SL added, enabling the estimation of SL concentrations in the samples. Chromatographic data and mass spectra were analyzed using AB Sciex Analyst software. The data are presented as the means of three or more biological replicates. In rare cases, due to compromised plant health, only two biological replicates were obtained.

CLA and 16-OH-CLA transport in Arabidopsis

A. thaliana seedlings of *cyp722a-1* mutant and WT Col-0 were grown in vermiculite for 30 days. Subsequently, each plant was grown separately and hydroponically for 7 days and then WT Col-0 was treated with 1 mM fluridone solution to inhibit SL production. Once SL production was confirmed to have ceased in wild type, CLA (1 μM) or 16-OH-CLA (1 μM) was supplemented into the hydroponic medium of both *cyp722a-1* mutant and WT Col-0.

After 18 hours of treatment, the shoots were excised 2 cm above the shoot/root junction to prevent possible contamination from the media. The shoot tissues (approximately 3 g fresh weight) were then extracted with acetone at 4°C for 24 hours. Following extraction, the tissues were removed by filtration, and the acetone was evaporated under vacuum. The identification of CLA and 16-OH-CLA was performed using LC-ESI-MS/MS with a differential mobility separation (DMS) spectrometer (QTRAP 5500 with SelexION System; AB Sciex, Japan). In addition to the MRM analysis parameters for CLA and 16-OH-CLA, the ion mobility analysis conditions were further optimized. The Separation Voltage (SV) was set to 3800 V and the Compensation Voltage (CoV) to −3.4 for CLA, while for 16-OH-CLA, the SV was set to 3500 V and the CoV to −16.9. This analytical method not only allows for the specific detection of the target compounds but also achieves a sensitivity more than 10 times greater than that of conventional MRM analysis.

Branching assay with strigolactone treatments

Seeds were frozen at −80°C for 24 hours, surface-sterilized, and sown on 0.5× Murashige-Skoog media. Seeds were stratified in the dark at 4°C for 3 days and then placed under white light (~110 μmol m^{-2} s^{-1}) with 16 hours light/8 hours dark photoperiod at ~21° to 24°C. Seedlings were transplanted into Sungro Professional Growing Mix as described above. After 15 to 18 days under white light, sites of axillary bud formation were treated with 10 μl of solvent control, 10 μM *rac*-GR24, or 10 μM 16-OH-CLA. All treatments were 0.5% (v/v) acetone. Plants were observed daily for anthesis. Treatments were performed every 2 days and axillary branches longer than 6 mm were counted at 14 days post-anthesis.

Hypocotyl elongation assay

Seeds were surface-sterilized and plated on 0.5× Murashige-Skoog media with MES buffer and vitamins (pH 5.8) with 0.8% Bacto Agar (BD). Media was supplemented with equal volumes

(0.5% (v/v) acetone) of solvent control, 16-OH-CLA, or *rac*-GR24. Seeds were stratified in the dark at 4°C for 3 days and then placed in a HiPoint DCI-700 LED Z4 growth chamber to grow at 21 °C under white light (150 μmol m^{-2} s^{-1}) for 3 hours, dark for 21 hours, and red light (30 μmol m^{-2} s^{-1}) for 4 days. Hypocotyl lengths were measured from photographs of seedlings with ImageJ (NIH).

Ratiometric SMXL7 reporter assay in N. benthamiana

pRATIO3212-SMXL7 + p19 (OD_{600} 0.6) was transiently expressed via agroinfiltration in leaves of three-week-old *N. benthamiana* UC Davis WT or *Nbd14a,b* plants, as described previously (*39*, *57*). After 3 days, leaf discs were measured for adequate reference protein expression (3× $Venus_{blank}$). 24 leaf discs were excised from each adequately expressing leaf and were treated with equal volumes (0.5% (v/v) acetone) of solvent control, 10 μM 16-OH-CLA, or 10 μM *rac*-GR24 for 16 to 18 hours before fluorescence analysis in a CLARIOstar microplate reader (BMG Labtech) (*39*, *40*, *58*). Each data point represents the average ratio of background-subtracted fluorescence from the treated discs excised from one leaf.

Branching and shoot height assay

Seeds were frozen at −80°C for 24 hours, surface-sterilized, and sown on 0.5× Murashige-Skroog media. Seeds were stratified in the dark at 4°C for 3 days and then placed under white light (~110 μmol m^{-2} s^{-1}) with 16 hours light/8 hours dark photoperiod at ~21° to 24°C. Seedlings were transplanted into Sungro Professional Growing Mix as described above. Plants were observed daily for anthesis. At 14 and 28 days post-anthesis, axillary branches longer than 6 mm were counted and shoot height was measured from the base of the rosette to the end of the longest shoot.

Quantitative reverse transcription PCR

Col-0 seeds were surface sterilized and transplanted to growth plugs containing ½ MS + 0.8% Difco Bacto agar and cold, dark stratified (4°C) for 3 days in a covered container. The container was placed under white light (~110 μmol m^{-2} s^{-1}) with 16 hours light/8 hours dark photoperiod at ~21° to 24°C for 14 days before being transferred to hydroponic containers containing Hoagland's No. 2 Basal Salt Media without ammonium phosphate (HOP02, Caisson Laboratories). Both containers were supplemented with ammonium phosphate monobasic (115.15 g/liter) and MES (0.25 g/liter). The media was pH'ed to 5.7 to 5.8. The hydroponic containers were aerated for five minutes every 25 min. At 20 days, media was exchanged with either ammonium phosphate-supplemented HOP02 media or HOP02 media. After 7 days, root and shoot tissues from 4 biological replicates (n = 4 pools of two plants) in both conditions were harvested in liquid nitrogen with a mortar and pestle. Shoot samples included the entirety of above-ground tissue: rosette, primary branch, axillary buds, and flowers. RNA samples were extracted with the Monarch Total RNA Miniprep Kit (T2010S, NEB), which included an on-column DNAse treatment. CDNA was synthesized with the Verso cDNA synthesis Kit (AB1453, ThermoFisher) using both Oligo-dT and random hexamers. Quantitative SYBER Green PCR was performed with the Luna Universal qPCR Master Mix (M3003, NEB) and the CFX384 Touch Real-Time PCR Detection System (Bio-Rad). Reactions were performed by using the following thermocycling conditions: an initial denaturation at 95°C for 3 min, followed by 39 cycles of denaturation at 95°C for 15 s and extension at 60°C for 30 s with a plate read at the end of each cycle. The melt curve analysis was conducted from 65°C to 95°C in 5-s increments, with plate reads at each step. Four biological and three technical replicates were analyzed. The relative expression was calculated against the housekeeping gene, *CLATHRIN ADAPTOR COMPLEX SUBUNIT (CACS)* CACS using the Pfaffl method. The nitrogen starvation experiment was conducted with the following adjustments. At 6 days, seedlings were transferred to hydroponic containers containing either ammonium phosphate-supplemented HOP02 media or nitrogen-free HOP03 media. The pH of the media was adjusted to 5.7-5.8 and replaced after two weeks. After 17 days in either nitrogen replete or deplete media, shoot tissues from 4 biological replicates (n = 4 individual plants) in both conditions were harvested in liquid nitrogen.The following primer pairs were used in this study, and their calculated efficiencies are included: *MAX3*, 5′-TCGTTGGTGAGCCCATGTTTGTC-3′ and 5′-TCTCCACCGAAACCGCATACTC-3′ (102%); *MAX4*, 5′-GAAAGATACCCACTTGGCTGAATG-3′ and 5′-TGTGGAGTAGCCGTCGAAGAG-3′ (100%); *MAX1*, 5′-CTATTTTCAGATTTCAGATGGGGAGGC-3′ and 5′-CCAACTTCTCTGCAAAGCTCTGC-3′ (97%); *CYP722A*, 5′-AACAGCGAAGGCTTCTAC-3′ and 5′-CTTGTCCTAAAGCAACTACCGTACC-3′ (104%); *CLAMT*, 5′-CCCTGAAAACACCATCCACT-3′ and 5′-TATGGACTTGCCTTGCTCGT-3′ (105%); *LBO*, 5′-CCCAAACTATGGCCCTCTAAACC-3′ and 5′-CCCCAAACATTTCCTCAAATCTCTCTTC-3′ (96%); *Pht1;8*, 5′-ACTATGGGAAGATCGTTAGAGGAG-3′ and 5′-AAAGTGCTCACGGAGGATTGC-3′ (93%); *NRT2.5*, 5′-CTCCTCCCTGTTATCCGTGAAA-3′ and 5′-AGACGAAAGTGGCGAGAGAGAA-3′ (96%); *CACS*, 5′-ACTCAGGAAGGTGTACGGTCA-3′ and 5′-TGCATTTGGAACAGGTTTGT-3′ (101%).

Phylogenetic analysis

CYP722 and CYP733 protein sequences were collected and identified through reciprocal best-BLAST match searches of Phytozome, NCBI, and the 1000 Plants Initiative (*59*–*61*). Sequences alignments were performed in MEGA 11 using the MUSCLE multiple sequence alignment algorithms (*62*). The multiple sequence alignment was trimmed using ClipKIT "kpic-smart-gap" (*63*). 295 out of 857 positions were trimmed. The phylogenetic tool IQ TREE inferred the evolutionary history using the Maximum Likelihood method and JTT matrix-based model (*64*). The tree with the highest log likelihood was selected. The Free Rate model was used to estimate evolutionary rate differences among sites (eight categories). This analysis involved 209 amino acid sequences. There was a total of 562 positions in the final dataset. Bootstrap values were calculated using UltraFast (10,000 iterations). Tree search settings were 0.5 perturbation strength and 100 iterations to stop. Trees were viewed in MEGA11.

Statistical analysis

Statistical analysis was performed in Graphpad Prism (version 10). Relative expression of SL biosynthesis genes (Fig. 2B and fig. S14) was measured with ordinary two-way analysis of variance (ANOVA) and Šídák's multiple comparisons test: compare within each gene. Branching treatment (Fig. 3A): Ordinary One-Way ANOVA: Gaussian distribution, unpaired, with pre-selected pairs of columns *max3-9* genotype only. Sidâk's multiple comparisons test of with single pooled variance. Hypocotyl Treatment Assay (Figs. 3B and 5A and fig. S19): Ordinary Two-Way ANOVA: unpaired, compare columns within each genotype. Tukey multiple comparisons. SMXL7 Degradation Tobacco Assay (Fig. 3C): Ordinary Two-Way ANOVA: unpaired, compare within each genotype. Tukey multiple comparisons. Branching and shoot height (Fig. 4 and figs. S21 and S22): Welch and Brown-Forsythe ANOVA or Ordinary One-Way ANOVA was used depending on the outcome of Levene's test for equality of variances. Gaussian distribution, unpaired, compare the mean of each column with the mean of every other column. Post-hoc for Welch ANOVA: Dunnett's T3 multiple comparisons test with individual variances computed for each comparison. Post-hoc for ordinary ANOVA: Tukey's multiple comparisons test with a single pooled variance. All outlier tests used ROUT Q = 1%.

Modeling and docking of CLA into LjCYP722C1 and CjCYP722A

The AlphaFold2 models of the full-length LjCYP722C1 and CjCYP722A proteins were utilized to predict the binding mode of CLA within their active sites. Both the protein and CLA were prepared and saved as PDBQT files. A grid box was generated using the Graphical User Interface in AutoDock Tools (ADT), with Kollman charges and polar hydrogens added to the proteins. The grid box dimensions were set to 52 by 50 by 48 *xyz* points with a grid spacing of 0.375Å, and the grid center was defined at coordinates x = 1.048, y = 4.1 and

z = −0.568. Docking was carried out using AutoDock Vina with the prepared ligand and protein files from ADT (*65*, *66*). The pose with the lowest binding energy was selected for further structural analysis, and all structural analysis and figure generation were carried out using PyMOLv3.0.

Detailed engineering strategies to enhance 5DS production

First, we examined different variants of D27, MAX1, and CYP722C for higher efficiency in synthesizing 5DS. D27 natural variants from a diversity of plant species across different clades from primitive vascular plants to flowering plants were selected for screening. The original OsD27 was replaced with a total of five different D27 variants, alongside the expression of *N*-terminal truncated CCD7 and CCD8 from *A. thaliana* (trAtCCD7 and trAtCCD8) and AtMAX1 in the CLA-producing microbial consortium (ECL1/YSL1, generating ECL2-6/YSL1, fig. S4A and table S2). CLA production from each consortium was estimated and used to evaluate the activities of different D27 variants. The D27 ortholog from *Physcomitrium patens* (PhpD27) exhibited the highest production of CLA, a 0.94-fold enhancement in comparison to OsD27 (fig. S4A). We also evaluated the activities of six additional variants of MAX1 and found that MAX1 from *Eucalyptus grandis* (EgMAX1) exhibited a 2.18-fold increase of CLA production compared to the original AtMAX1 (ECL2/YSL8-13, fig. S4B and table S2). Similarly, five Group II CYP722C variants were assessed, and CYP722C from *Ricinus communis* (RcCYP722C2) showed the highest efficiency toward the synthesis of 5DS (ECL2/YSL15-19) (fig. S4C and table S2). Taken together, the 5DS-producing ECL2/YSL16 expressing PhpD27, EgMAX1, and RcCYP722C2 achieved a 5DS titer of 141.9 μg/liter when the *E. coli* strain was induced with 0.2 mM IPTG at 25°C for 48 hours, which showcased a remarkable 15-fold enhancement compared to the original 5DS-producing ECL1/YSL14 (8.85 μg/liter) (Fig. 2A and table S2). The culture and extraction method used in this study differs from what was used in the highest reported titer (*21*). Therefore, the initial 5DS titer is lower than the previously reported value of 47.3 μg/liter.

As CLA was barely detectable after 2-day fermentation in ECL2/YSL16 (fig. S4C and table S2) along with almost complete CL consumption, the conversion of CL to SLs was no longer rate-limiting. To further enhance the 5DS titer, it is necessary to enhance CL production. First, we expressed D27, CCD7, and CCD8 under different plasmid systems (table S3). Utilization of a two-plasmid system coexpressing PhpD27, trAtCCD7, and trAtCCD8 from the low-copy number vector pCDFDuet-1 leads to a 0.82-fold increase in CLA production as well as a 16.5-fold elevation in CL accumulation, in contrast to the original three-plasmid system in ECL2 (fig. S5A and table S2). We further improved the activity of D27, a pivotal enzyme catalyzing the initial conversion of all-*trans*-β-carotene into 9-*cis*-β-carotene in the SL biosynthesis. According to prior engineering efforts, *N*-terminal modification could be used as an effective strategy to enhance the performance of enzymes (*67*, *68*). Two functional tags, 28 amino acid tag (28aa) (*69*) and transmembrane tag (residues 1 to 48) derived from SohB ($SohB^{1-48}$) (*70*), were thus selected and fused to the *N*-terminus of PhpD27, respectively. Removal of the putative plastid transit peptide was also applied to PhpD27 (trPhpD27). The fusion of the SohB transmembrane tag at the *N*-terminus of PhpD27 ($SohB^{1-48}$-PhpD27) resulted in a substantial improvement in the CL production (ECL12/YSL12) (fig. S5B and table S2). Furthermore, given that the expression of D27, CCD7, and CCD8 is regulated by the *T7* promoter induced with IPTG (originally 0.2 mM), we tuned the protein expression levels in ECL12 by adjusting the IPTG concentration from 0.05 to 0.5 mM. The results demonstrated that when ECL12 was induced with 0.5 mM IPTG, the highest CLA production was observed (fig. S5C). When YSL16 was cocultured with ECL12 that was induced with 0.5 mM IPTG, 5DS was produced at a titer of 175.8 μg/liter, 0.24-fold greater than when cocultured with ECL2 that was induced with 0.2 mM IPTG (Fig. 1D and table S2).

The accumulation of CL in ECL12/YSL12 implies that it is necessary to optimize the performance of the CL-consuming yeast strains (fig. S5C and table S2). Previous studies demonstrate that the yeast endogenous CPR (ScCPR) encoded by *ncp1* possessed low compatibility with plant CYPs and might interfere with the electron transfer between CYTOCHROME P450 REDUCTASE 1 (ATR1) and plant derived CYPs (*71*, *72*). Accordingly, *ncp1* was replaced with *ATR1* gene in CEN.PK2-1D, yielding YSL20 (table S2). The efficiency of 5DS biosynthesis was evaluated between CEN.PK2-1D expressing ATR1, EgMAX1 and RcCYP722C2 (YSL16) (table S2) and YSL20 expressing EgMAX1 and RcCYP722C2 (YSL21) (table S2), both of which were cocultured with ECL12. The 5DS titer in ECL12/YSL21 achieved a 2.3-fold enhancement at 537.2 μg/liter compared to ECL12/YSL16, reflecting the improved catalytic efficiency of CYPs in yeast (fig. S6A). We also speculated that the amount of biocatalyst, such as MAX1 or CYP722C, was a limit, and thus elevating the biocatalyst concentration could further enhance CL conversion. Therefore, we integrated up to three copies of *EgMAX1* onto the genome of YSL20, generating YSL22-24 (table S2). It was shown that increasing *EgMAX1* copies positively correlates with the conversion of CLA from CL, though this trend diminished after incorporating a third *EgMAX1* copy (ECL12/YSL24) (fig. S6B and table S2). Similarly, different copies of *RcCYP722C2* were introduced into YSL22-24 separately to determine the optimal expression levels of *EgMAX1* and *RcCYP722C2* for the bioproduction of 5DS. Among all the microbial consortia established (ECL12/YSL26-28, ECL12/YSL30-32, ECL12/YSL34-35) (table S2), ECL12/YSL31 expressing two copies of both *EgMAX1* and *RcCYP722C2* genes exhibited the highest 5DS titer at 1.12 mg/liter (fig. S6C), more than 120-fold enhancement from the original titer.

REFERENCES AND NOTES

1. K. Yoneyama, P. B. Brewer, Strigolactones, how are they synthesized to regulate plant growth and development? *Curr. Opin. Plant Biol.* **63**, 102072 (2021). doi: 10.1016/j.pbi.2021.102072; pmid: 34198192
2. A. Temmerman, A. Guillory, S. Bonhomme, S. Goormachtig, S. Struk, Masks start to drop: Suppressor of MAX2 1-like proteins reveal their many faces. *Front. Plant Sci.* **13**, 887232 (2022). doi: 10.3389/fpls.2022.887232; pmid: 35645992
3. M. T. Waters, C. Gutjahr, T. Bennett, D. C. Nelson, Strigolactone signaling and evolution. *Annu. Rev. Plant Biol.* **68**, 291–322 (2017). doi: 10.1146/annurev-arplant-042916-040925; pmid: 28125281
4. J. Clark, T. Bennett, Cracking the enigma: Understanding strigolactone signalling in the rhizosphere. *J. Exp. Bot.* **75**, 1159–1173 (2024). doi: 10.1093/jxb/erad335; pmid: 37623748
5. D. C. Nelson, The mechanism of host-induced germination in root parasitic plants. *Plant Physiol.* **185**, 1353–1373 (2021). doi: 10.1093/plphys/kiab043; pmid: 33793958
6. S. Ogawa *et al.*, Strigolactones are chemoattractants for host tropism in Orobanchaceae parasitic plants. *Nat. Commun.* **13**, 4653 (2022). doi: 10.1038/s41467-022-32314-z; pmid: 35970835
7. T. Wakabayashi *et al.*, Direct conversion of carlactonoic acid to orobanchol by cytochrome P450 CYP722C in strigolactone biosynthesis. *Sci. Adv.* **5**, eaax9067 (2019). doi: 10.1126/sciadv.aax9067; pmid: 32064317
8. K. Yoneyama *et al.*, Which are the major players, canonical or non-canonical strigolactones? *J. Exp. Bot.* **69**, 2231–2239 (2018). doi: 10.1093/jxb/ery090; pmid: 29522151
9. S. Ito *et al.*, Canonical strigolactones are not the major determinant of tillering but important rhizospheric signals in rice. *Sci. Adv.* **8**, eadd1278 (2022). doi: 10.1126/sciadv.add1278; pmid: 36322663
10. G. E. Chen *et al.*, Disruption of the rice *4-DEOXYOROBANCHOL HYDROXYLASE* unravels specific functions of canonical strigolactones. *Proc. Natl. Acad. Sci. U.S.A.* **120**, e2306263120 (2023). doi: 10.1073/pnas.2306263120; pmid: 37819983
11. R. Yao *et al.*, DWARF14 is a non-canonical hormone receptor for strigolactone. *Nature* **536**, 469–473 (2016). doi: 10.1038/nature19073; pmid: 27479325
12. A. de Saint Germain *et al.*, An histidine covalent receptor and butenolide complex mediates strigolactone perception. *Nat. Chem. Biol.* **12**, 787–794 (2016). doi: 10.1038/nchembio.2147; pmid: 27479744
13. T. Nomura, Y. Seto, J. Kyozuka, Unveiling the complexity of strigolactones: Exploring structural diversity, biosynthesis pathways, and signaling mechanisms. *J. Exp. Bot.* **75**, 1134–1147 (2024). doi: 10.1093/jxb/erad412; pmid: 37877933
14. A. Alder *et al.*, The path from β-carotene to carlactone, a strigolactone-like plant hormone. *Science* **335**, 1348–1351 (2012). doi: 10.1126/science.1218094; pmid: 22422982
15. Y. Zhang *et al.*, Rice cytochrome P450 MAX1 homologs catalyze distinct steps in strigolactone biosynthesis. *Nat. Chem. Biol.* **10**, 1028–1033 (2014). doi: 10.1038/nchembio.1660; pmid: 25344813
16. S. Wu *et al.*, Identification of a Prunus MAX1 homolog as a unique strigol synthase. *New Phytol.* **239**, 1819–1833 (2023). doi: 10.1111/nph.19052; pmid: 37292030
17. K. Mashiguchi *et al.*, A carlactonoic acid methyltransferase that contributes to the inhibition of shoot branching in *Arabidopsis*. *Proc. Natl. Acad. Sci. U.S.A.* **119**, e2111565119 (2022). doi: 10.1073/pnas.2111565119; pmid: 35344437
18. T. Wakabayashi *et al.*, Specific methylation of (11R)-carlactonoic acid by an *Arabidopsis* SABATH methyltransferase. *Planta* **254**, 88 (2021). doi: 10.1007/s00425-021-03738-6; pmid: 34586497
19. R. Yang *et al.*, LATERAL BRANCHING OXIDOREDUCTASE, one novel target gene of Squamosa Promoter Binding Protein-like 2, regulates tillering in switchgrass. *New Phytol.* **235**, 563–575 (2022). doi: 10.1111/nph.18140; pmid: 35383390

20. N. Mori, T. Nomura, K. Akiyama, Identification of two oxygenase genes involved in the respective biosynthetic pathways of canonical and non-canonical strigolactones in Lotus japonicus. *Planta* **251**, 40 (2020). doi: 10.1007/s00425-019-03332-x; pmid: 31907631
21. S. Wu *et al*., Establishment of strigolactone-producing bacterium-yeast consortium. *Sci. Adv.* **7**, eabh4048 (2021). doi: 10.1126/sciadv.abh4048; pmid: 34533983
22. T. Wakabayashi *et al*., CYP722C from Gossypium arboreum catalyzes the conversion of carlactonoic acid to 5-deoxystrigol. *Planta* **251**, 97 (2020). doi: 10.1007/s00425-020-03390-6; pmid: 32306106
23. M. Homma *et al*., Insights into stereoselective ring formation in canonical strigolactone: Identification of a dirigent domain-containing enzyme catalyzing orobanchol synthesis. *Proc. Natl. Acad. Sci. U.S.A.* **121**, e2313683121 (2024). doi: 10.1073/pnas.2313683121; pmid: 38905237
24. S. Wu, Y. Li, A unique sulfotransferase-involving strigolactone biosynthetic route in sorghum. *Front. Plant Sci.* **12**, 793459 (2021). doi: 10.3389/fpls.2021.793459; pmid: 34970291
25. A. Yoda *et al*., Strigolactone biosynthesis catalyzed by cytochrome P450 and sulfotransferase in sorghum. *New Phytol.* **232**, 1999–2010 (2021). doi: 10.1111/nph.17737; pmid: 34525227
26. C. H. Walker, K. Siu-Ting, A. Taylor, M. J. O'Connell, T. Bennett, Strigolactone synthesis is ancestral in land plants, but canonical strigolactone signalling is a flowering plant innovation. *BMC Biol.* **17**, 70 (2019). doi: 10.1186/s12915-019-0689-6; pmid: 31488154
27. Y. Li *et al*., Complete biosynthesis of noscapine and halogenated alkaloids in yeast. *Proc. Natl. Acad. Sci. U.S.A.* **115**, E3922–E3931 (2018). doi: 10.1073/pnas.1721469115; pmid: 29610307
28. D. W. Bolen, Protein stabilization by naturally occurring osmolytes. *Methods Mol. Biol.* **168**, 17–36 (2001). doi: 10.1385/1-59259-193-0:017; pmid: 11357625
29. E. T. Trevisol, A. D. Panek, S. C. Mannarino, E. C. Eleutherio, The effect of trehalose on the fermentation performance of aged cells of *Saccharomyces cerevisiae*. *Appl. Microbiol. Biotechnol.* **90**, 697–704 (2011). doi: 10.1007/s00253-010-3053-x; pmid: 21243352
30. S. Abe *et al*., Carlactone is converted to carlactonoic acid by MAX1 in Arabidopsis and its methyl ester can directly interact with AtD14 in vitro. *Proc. Natl. Acad. Sci. U.S.A.* **111**, 18084–18089 (2014). doi: 10.1073/pnas.1410801111; pmid: 25425668
31. K. Yoneyama *et al*., Hydroxyl carlactone derivatives are predominant strigolactones in *Arabidopsis*. *Plant Direct* **4**, e00219 (2020). doi: 10.1002/pld3.219; pmid: 32399509
32. E. A. Dun, P. B. Brewer, E. M. J. Gillam, C. A. Beveridge, Strigolactones and shoot branching: What is the real hormone and how does it work? *Plant Cell Physiol.* **64**, 967–983 (2023). doi: 10.1093/pcp/pcad088; pmid: 37526426
33. M. A. Naseer *et al*., Strigolactones: A promising tool for nutrient acquisition through arbuscular mycorrhizal fungi symbiosis and abiotic stress tolerance. *Plant Physiol. Biochem.* **215**, 109057 (2024). doi: 10.1016/j.plaphy.2024.109057; pmid: 39173365
34. D. Nelson, D. Werck-Reichhart, A P450-centric view of plant evolution. *Plant J.* **66**, 194–211 (2011). doi: 10.1111/j.1365-313X.2011.04529.x; pmid: 21443632
35. M. T. Waters, D. C. Nelson, Karrikin perception and signalling. *New Phytol.* **237**, 1525–1541 (2023). doi: 10.1111/nph.18598; pmid: 36333982
36. L. Wang *et al*., Strigolactone and karrikin signaling pathways elicit ubiquitination and proteolysis of SMXL2 to regulate hypocotyl elongation in *Arabidopsis*. *Plant Cell* **32**, 2251–2270 (2020). doi: 10.1105/tpc.20.00140; pmid: 32358074
37. Q. Li *et al*., The strigolactone receptor D14 targets SMAX1 for degradation in response to GR24 treatment and osmotic stress. *Plant Commun.* **3**, 100303 (2022). doi: 10.1016/j.xplc.2022.100303; pmid: 35529949
38. L. Wang *et al*., Strigolactone signaling in arabidopsis regulates shoot development by targeting D53-Like SMXL repressor proteins for ubiquitination and degradation. *Plant Cell* **27**, 3128–3142 (2015). doi: 10.1105/tpc.15.00605; pmid: 26546446
39. A. R. F. White, J. A. Mendez, A. Khosla, D. C. Nelson, Rapid analysis of strigolactone receptor activity in a *Nicotiana benthamiana dwarf14* mutant. *Plant Direct* **6**, e389 (2022). doi: 10.1002/pld3.389; pmid: 35355884
40. A. Khosla, C. Rodriguez-Furlan, S. Kapoor, J. M. Van Norman, D. C. Nelson, A series of dual-reporter vectors for ratiometric analysis of protein abundance in plants. *Plant Direct* **4**, e00231 (2020). doi: 10.1002/pld3.231; pmid: 32582876
41. J. Jumper *et al*., Highly accurate protein structure prediction with AlphaFold. *Nature* **596**, 583–589 (2021). doi: 10.1038/s41586-021-03819-2; pmid: 34265844
42. X. Xie, Structural diversity of strigolactones and their distribution in the plant kingdom. *J. Pestic. Sci.* **41**, 175–180 (2016). doi: 10.1584/jpestics.J16-02; pmid: 30363158
43. M. H. Vinde *et al*., Ancestral sequence reconstruction of the CYP711 family reveals functional divergence in strigolactone biosynthetic enzymes associated with gene duplication events in monocot grasses. *New Phytol.* **235**, 1900–1912 (2022). doi: 10.1111/nph.18285; pmid: 35644901
44. K. Kodama *et al*., An ancestral function of strigolactones as symbiotic rhizosphere signals. *Nat. Commun.* **13**, 3974 (2022). doi: 10.1038/s41467-022-31708-3; pmid: 35803942
45. D. G. Gibson *et al*., Enzymatic assembly of DNA molecules up to several hundred kilobases. *Nat. Methods* **6**, 343–345 (2009). doi: 10.1038/nmeth.1318; pmid: 19363495
46. X. Xie, K. Yoneyama, T. Nomura, K. Yoneyama, *Strigolactones: Methods and Protocols* (Springer, 2021), pp. 3–12, 10.1007/978-1-0716-1429-7_1.
47. J. Booker *et al*., MAX3/CCD7 is a carotenoid cleavage dioxygenase required for the synthesis of a novel plant signaling molecule. *Curr. Biol.* **14**, 1232–1238 (2004). doi: 10.1016/j.cub.2004.06.061; pmid: 15268852
48. M. T. Waters *et al*., Specialisation within the DWARF14 protein family confers distinct responses to karrikins and strigolactones in *Arabidopsis*. *Development* **139**, 1285–1295 (2012). doi: 10.1242/dev.074567; pmid: 22357928
49. S. Toh, D. Holbrook-Smith, M. E. Stokes, Y. Tsuchiya, P. McCourt, Detection of parasitic plant suicide germination compounds using a high-throughput *Arabidopsis* HTL/KAI2 strigolactone perception system. *Chem. Biol.* **21**, 988–998 (2014). doi: 10.1016/j.chembiol.2014.07.005; pmid: 25126711
50. J. M. Alonso *et al*., Genome-wide insertional mutagenesis of *Arabidopsis thaliana*. *Science* **301**, 653–657 (2003). doi: 10.1126/science.1086391; pmid: 12893945
51. H. Liu *et al*., CRISPR-P 2.0: An improved CRISPR-Cas9 tool for genome editing in plants. *Mol. Plant* **10**, 530–532 (2017). doi: 10.1016/j.molp.2017.01.003; pmid: 28089950
52. J. Angulo *et al*., CRISPR/Cas9 mutagenesis of the *Arabidopsis* GROWTH-REGULATING FACTOR (GRF) gene family. *Front. Genome Ed.* **5**, 1251557 (2023). doi: 10.3389/fgeed.2023.1251557; pmid: 37908969
53. Z. P. Wang *et al*., Egg cell-specific promoter-controlled CRISPR/Cas9 efficiently generates homozygous mutants for multiple target genes in *Arabidopsis* in a single generation. *Genome Biol.* **16**, 144 (2015). doi: 10.1186/s13059-015-0715-0; pmid: 26193878
54. S. J. Clough, A. F. Bent, Floral dip: A simplified method for Agrobacterium-mediated transformation of *Arabidopsis thaliana*. *Plant J.* **16**, 735–743 (1998). doi: 10.1046/j.1365-313x.1998.00343.x; pmid: 10069079
55. C. Hodgens, Z. L. Nimchuk, J. J. Kieber, indCAPS: A tool for designing screening primers for CRISPR/Cas9 mutagenesis events. *PLOS ONE* **12**, e0188406 (2017). doi: 10.1371/journal.pone.0188406; pmid: 29141013
56. T. Nakagawa *et al*., Improved Gateway binary vectors: High-performance vectors for creation of fusion constructs in transgenic analysis of plants. *Biosci. Biotechnol. Biochem.* **71**, 2095–2100 (2007). doi: 10.1271/bbb.70216; pmid: 17690442
57. A. Khosla *et al*., Structure-function analysis of SMAX1 reveals domains that mediate its karrikin-induced proteolysis and interaction with the receptor KAI2. *Plant Cell* **32**, 2639–2659 (2020). doi: 10.1105/tpc.19.00752; pmid: 32434855
58. A. Khosla, D. C. Nelson, Ratiometric measurement of protein abundance after transient expression of a transgene in *Nicotiana benthamiana*. *Bio Protoc.* **10**, e3747 (2020). doi: 10.21769/BioProtoc.3747; pmid: 33659407
59. One Thousand Plant Transcriptomes Initiative, One thousand plant transcriptomes and the phylogenomics of green plants. *Nature* **574**, 679–685 (2019). doi: 10.1038/s41586-019-1693-2; pmid: 31645766
60. D. M. Goodstein *et al*., Phytozome: A comparative platform for green plant genomics. *Nucleic Acids Res.* **40** (D1), D1178–D1186 (2012). doi: 10.1093/nar/gkr944; pmid: 22110026
61. E. J. Carpenter *et al*., Access to RNA-sequencing data from 1,173 plant species: The 1000 Plant Transcriptomes Initiative (1KP). *Gigascience* **8**, giz126 (2019). doi: 10.1093/gigascience/giz126; pmid: 31644802
62. K. Tamura, G. Stecher, S. Kumar, MEGA11: Molecular Evolutionary Genetics Analysis Version 11. *Mol. Biol. Evol.* **38**, 3022–3027 (2021). doi: 10.1093/molbev/msab120; pmid: 33892491
63. J. L. Steenwyk, T. J. Buida III, Y. Li, X. X. Shen, A. Rokas, ClipKIT: A multiple sequence alignment trimming software for accurate phylogenomic inference. *PLOS Biol.* **18**, e3001007 (2020). doi: 10.1371/journal.pbio.3001007; pmid: 33264284
64. J. Trifinopoulos, L. T. Nguyen, A. von Haeseler, B. Q. Minh, W-IQ-TREE: A fast online phylogenetic tool for maximum likelihood analysis. *Nucleic Acids Res.* **44**, W232-5 (2016). doi: 10.1093/nar/gkw256; pmid: 27084950
65. J. Eberhardt, D. Santos-Martins, A. F. Tillack, S. Forli, AutoDock Vina 1.2.0: New docking methods, expanded force field, and Python bindings. *J. Chem. Inf. Model.* **61**, 3891–3898 (2021). doi: 10.1021/acs.jcim.1c00203; pmid: 34278794
66. O. Trott, A. J. Olson, AutoDock Vina: Improving the speed and accuracy of docking with a new scoring function, efficient optimization, and multithreading. *J. Comput. Chem.* **31**, 455–461 (2010). doi: 10.1002/jcc.21334; pmid: 19499576
67. B. W. Biggs *et al*., Overcoming heterologous protein interdependency to optimize P450-mediated Taxol precursor synthesis in Escherichia coli. *Proc. Natl. Acad. Sci. U.S.A.* **113**, 3209–3214 (2016). doi: 10.1073/pnas.1515826113; pmid: 26951651
68. A. Zhou, K. Zhou, Y. Li, Rational design strategies for functional reconstitution of plant cytochrome P450s in microbial systems. *Curr. Opin. Plant Biol.* **60**, 102005 (2021). doi: 10.1016/j.pbi.2021.102005; pmid: 33647811
69. M. H. Nørholm *et al*., Improved production of membrane proteins in *Escherichia coli* by selective codon substitutions. *FEBS Lett.* **587**, 2352–2358 (2013). doi: 10.1016/j.febslet.2013.05.063; pmid: 23769986
70. U. Christensen *et al*., De-bugging and maximizing plant cytochrome P450 production in *Escherichia coli* with C-terminal GFP fusions. *Appl. Microbiol. Biotechnol.* **101**, 4103–4113 (2017). doi: 10.1007/s00253-016-8076-5; pmid: 28204885
71. N. Milne *et al*., Metabolic engineering of *Saccharomyces cerevisiae* for the de novo production of psilocybin and related tryptamine derivatives. *Metab. Eng.* **60**, 25–36 (2020). doi: 10.1016/j.ymben.2019.12.007; pmid: 32224264
72. T. Liu *et al*., Efficient production of vindoline from tabersonine by metabolically engineered *Saccharomyces cerevisiae*. *Commun. Biol.* **4**, 1089 (2021). doi: 10.1038/s42003-021-02617-w; pmid: 34531512

ACKNOWLEDGMENTS

We thank S. Cutler (University of California, Riverside) and K. Zhou (National University of Singapore) for the helpful discussion and S. Xu and K. Wang for valuable feedback in the preparation of the manuscript. pAC-BETAipi was a gift from F. X. Cunningham Jr. (Addgene plasmid 53277; http://n2t.net/addgene:53277; RRID: Addgene_53277). **Funding:** This work was supported by the National Science Foundation (CAREER Award CBET-2144626 and CAREER Award CBET-2420331 to Y.L., IOS-1856741 and IOS-2329271 to D.C.N., CAREER Award 2047396 to N.S., and Research Traineeship Program Grant DGE-1922642 "Plants3D" to A.Z. and A.K.); USDA-NIFA (AFRI Predoctoral Fellowship 2023-67011-40396 to A.K.); Japan Science and Technology Agency (FOREST, JPMJFR22OF to K.Y.); Japan Society for the Promotion of Science (KAKENHI, 23K21177 to X.X.); and the Japan Science and Technology Agency (FOREST JPMJFR22OF to K.Y.). **Author contributions:** Conceptualization: X.X., D.C.N., and Y.L. Methodology: A.Z., A.K., S.W., K.Y., X.X., D.C.N., and Y.L. Investigation: A.Z., A.K., S.W., K.W., M.S., Y.I., K.Y., M.P., and X.X. Funding acquisition: A.K., K.Y., X.X., D.C.N., and Y.L. Project administration: Y.L. Supervision: X.X., D.C.N., and Y.L. Writing – original draft: A.Z., A.K., X.X., D.C.N., and Y.L. Writing – review and editing: A.Z., A.K., K.Y., M.P., N.S., X.X., D.C.N., and Y.L. **Competing interests:** A.Z., S.W., and Y.L. are inventors on a provisional patent application related to this work filed by University of California, Riverside (US provisional application No. 63/142,801, filed 28 January 2021, patent pending). The authors declare that they have no other competing interests. **Data and materials availability:** All data are available in the main text or the supplementary materials.

SUPPLEMENTARY MATERIALS

science.org/doi/10.1126/science.adp0779
Figs. S1 to S31
Tables S1 to S8
References (*73*–*77*)
MDAR Reproducibility Checklist

Submitted 7 March 2024; resubmitted 30 August 2024
Accepted 6 November 2024
10.1126/science.adp0779